University of Lisbon, Faculty of Medicine
Unit of Neurosciences, Institute of Molecular Medicine

The neuromuscular transmission of the SOD1(G93A) mouse model of Amyotrophic Lateral Sclerosis

Mariana Cúcio Rocha

Master in Neurosciences
Lisbon 2012

University of Lisbon, Faculty of Medicine
Unit of Neurosciences, Institute of Molecular Medicine

The neuromuscular transmission of the SOD1(G93A) mouse model of Amyotrophic Lateral Sclerosis

Mariana Cúcio Rocha

Supervised by:
Joaquim A. Ribeiro, MD, PhD
Paula Pousinha, PhD

Master in Neurosciences
Lisbon 2012

The printing of this thesis was approved by the Coordinating Committee of the Scientific Board of the Faculty of Medicine, University of Lisbon, on the October 23rd 2012, meeting.

A impressão desta dissertação foi aprovada pela Comissão Coordenadora do Conselho Científico da Faculdade de Medicina da Universidade de Lisboa em reunião de 23 de Outubro de 2012.

O trabalho experimental apresentado nesta tese foi realizado no Instituto de Farmacologia e Neurociências, Faculdade de Medicina e Unidade de Neurociências, Instituto de Medicina Molecular, sob orientação do Professor Doutor Joaquim Alexandre Ribeiro e Doutora Paula Pousinha.

The experimental work described in this thesis was performed at the Institute of Pharmacology and Neuroscience, Faculty of Medicine and Unit of Neurosciences, Institute of Molecular Medicine, under supervision of Professor Joaquim Alexandre Ribeiro and Professor Paula Pousinha.

Table of contents

Abbreviation list

ACh	Acetylcholine
AChE	Acetylcholinesterase
AChR	Acetylcholine receptor
ALS	Amyotrophic Lateral Sclerosis
ATP	Adenosine 5´-triphosphate
ChAT	Choline acethyltransferase
EPP	Endplate potential
GMEPP	Giant miniature endplate potential
IgGs	Immunoglobulins G
IP3	Inositol 1,4,5-triphosphate
LF	Latency-to-fall
MEPP	Miniature endplate potential
NMJ	Neuromuscular junction
QC	*Quantal content*
Rpm	Rotations-per-minute
SEM	Standard error mean
TNF	Tumor Necrosis Factor

Resumo

A Esclerose Lateral Amiotrófica (ELA), uma das doenças do neurónio motor mais comum, caracteriza-se pela perda selectiva de neurónios motores do tracto corticoespinhal. Vários estudos sugerem que a degeneração inicia-se na porção distal do axónio com uma progressão retrógrada. Assim, o presente trabalho teve como objectivo avaliar a transmissão sináptica na junção neuromuscular dos animais SOD1(G93A), nos períodos correspondentes às fases pré-sintomática e sintomática da ELA.

As experiências foram efectuadas em ratinhos transgénicos SOD1(G93A) e não transgénicos (WT), na fase pré-sintomática (4 a 6 semanas de idade) e fase sintomática (12 a 16 semanas de idade). Após o nascimento, os animais foram genotipados por *polymerase chain reaction* (PCR). Nas respectivas fases da doença, os animais foram testados no rotarod, e em seguida fizeram-se registos electrofisiologicos: potenciais de placa evocados (EPPs), potenciais de placa miniatura (MEPPs) e MEPPs gigantes (GMEPPs: MEPPs > 1mV). Os registos foram feitos em fibras musculares do diafragma inervado, paralisadas com µ-conotoxina GIIIB. O conteúdo quântico dos EPPs foi calculado através da razão entre a amplitude média dos EPPs e a amplitude média dos MEPPs.

Na fase pré-sintomática da doença, os ratos SOD1(G93A) não exibiram alterações na função motora a 10 rpm. Relativamente à transmissão neuromuscular, estes animais apresentaram um aumento significativo da amplitude média dos EPPs e do conteúdo quântico dos EPPs, quando comparados com os animais WT, sugerindo uma maior eficiência da transmissão neuromuscular nos animais SOD1(G93A). Para além disso, o aumento significativo da frequência de GMEPPs, o que pela literatura parece estar associado a uma desregulação dos níveis intracelulares de Ca^{2+}, e as alterações na amplitude e cinética dos MEPPs sugerem a existência de alterações ao nível da junção neuromuscular numa fase pré-sintomatica. Na fase sintomática, os animais SOD1(G93A) apresentaram um défice motor aos 10 rpm. Os registos electrofisiológicos revelaram a existência de dois grupos de junções neuromusculares nos ratos SOD1(G93A): SOD1a e SOD1b. O grupo SOD1a apresentou EPPs e MEPPs com amplitudes significativamente reduzidas bem como um *rise-time* dos MEPPs aumentado, quando comparado com os grupos SOD1b e WT, sugerindo um enfraquecimento da transmissão neuromuscular, nesse grupo. Pelo contrário, o grupo SOD1b apresentou uma transmissão neuromuscular semelhante tanto à dos animais SOD1(G93A) pré-sintomáticos, como também à dos WT com 12-14 semanas.

Em conclusão, este trabalho mostra que a transmissão neuromuscular dos animais SOD1(G93A) encontra-se aumentada na fase pré-sintomática. Na fase sintomática, a presença de uma população mista de junções neuromusculares é consistente com os ciclos de desinervação/ re-inervação, já descritos

noutros estudos. As alterações iniciais na transmissão neuromuscular dos animais SOD1(G93A) representam assim mais uma evidência que os mecanismos patológicos da ELA iniciam-se antes do aparecimento dos primeiros sintomas.

Abstract

Amyotrophic Lateral Sclerosis (ALS) is the most frequent adult-onset motor neuron disease and is characterized by a selective and progressive loss of motor neurons in the corticospinal tract. Growing evidence suggest that degeneration may begin at the distal axon proceeding in a dying-back pattern, increasing the need to focus on neuromuscular junction parameters. It seemed therefore of interest to investigate synaptic transmission at the neuromuscular junction (NMJ) in both pre- and symptomatic phases of the disease.

Experiments were performed in SOD1(G93A) mice and in non-transgenic littermates (WT) with 4-6 and 12-14 weeks-old, corresponding respectively to pre- and symptomatic phases. After birth, mice were genotyped through polymerase chain reaction (PCR). At the respective age, mice were submitted rotarod, then low-frequency (0.5 Hz) evoked endplate potentials (EPPs), miniature endplate potentials (MEPPs) and giant MEPPs (GMEPPs: MEPPs >1mV) were recorded from innervated diaphragm muscle fibers, paralyzed with μ-conotoxin GIIIB. The *quantal content* of EPPs was estimated as the ratio between EPPs amplitude and MEPPs amplitude.

In the pre-symptomatic phase, SOD1(G93A) mice did not present motor deficits on the rotarod at 10rpm. However, SOD1(G93A) mice exhibited a significant increase of the mean amplitude of EPPs together with an increase in the mean *quantal content* of EPPs, suggesting that more acetylcholine is being released into the synaptic cleft. Also, SOD1(G93A) mice presented a higher frequency of GMEPPs, suggestive of intracellular Ca^{2+} deregulation in nerve terminals. The observed increase in the mean amplitude of MEPPs and the decreased mean rise-time of MEPPs in SOD1(G93A) mice point as well to post-synaptic related changes. In symptomatic phase, SOD1(G93A) mice presented a lower motor balance and coordination. Electrophysiological data showed evidence for two NMJ groups in SOD1(G93A) mice: SOD1a and SOD1b. The SOD1a group presented both mean amplitude of EPPs and of MEPPs reduced. The mean rise-time of MEPPs was increased, when compared to WT and to SOD1b group, indicating an impairment in the neuromuscular transmission. In contrast, the neuromuscular transmission of SOD1b group was not different from age-matched WT or from the pre-symptomatic SOD1(G93A) mice.

Altogether these results clearly show that the neuromuscular transmission of SOD1(G93A) mice is enhanced in the pre-symptomatic phase. In the symptomatic phase our results are consistent with the hypothesis that the diaphragm of SOD1(G93A) mice are undergoing cycles of denervation/re-innervation supported by the mixed population of neuromuscular junctions. These early changes in the neuromuscular

transmission of SOD1(G93A) mice is a novel proof that the ALS associated events starts long before the symptoms appear.

Keywords: Amyotrophic Lateral Sclerosis, neuromuscular transmission, SOD1(G39A) mice

1 Introduction

1.1 Amyotrophic Lateral Sclerosis: the disease

1.1.1 Disease definition and primary features

Amyotrophic Lateral Sclerosis (ALS), also known as Charcot´s Sclerosis or Lou Gehrig´s disease, is the most common adult-onset motor neuron disease and the most frequent neurodegenerative disorder after Alzheimer and Parkinson diseases. Although its incidence is similar to that of multiple sclerosis (2-3 per 100,000 each year), its low prevalence of just 4-6 per 100,000 each year, owing to the poor prognosis, understates the impact of ALS (see Boillee et al., 2006 and Dion et al., 2009).

The primary disease hallmark is a selective and progressive degeneration of motor neurons in the corticospinal tracts. The consequent loss of upper motor neurons, which are found in the motor cortex, triggers spasticity and hyper-reflexia while that of lower motor neurons, present in the brainstem and spinal cord, leads to widespread muscle weakness, atrophy and paralysis. This disorder is diagnosed in midlife (usually between age 45 and 60) and patients die once denervation reaches the respiratory muscles and diaphragm, that is 1 to 5 years after symptoms onset (see Gonzalez de Aguilar et al., 2007).

Most cases (90%) do not present a hereditary pattern and are hence classified as sporadic ALS. Increasing evidence suggest the involvement of genetic factors, with susceptibility genes increasing the overall risk for neurodegeneration, as well of epigenetics. The remaining 10% are termed familial ALS and the disease is frequently inherited in an autosomal dominant manner. Over the past two decades, 13 genes and loci have been reported to predispose to ALS. However, both forms produce similar pathological and clinical hallmarks suggesting a common pathogenesis (see Boillee et al., 2006; Kiernan et al., 2011).

Despite many advances in investigative medicine over the past decades, there is no diagnostic test for ALS. Clinicians have to identify a combination of diagnostic features and classify patients into categories according to the level of diagnostic certainly, which is a method of detection with very poor sensitivity particularly in the early stages of the disease. Regarding the management of ALS, there is no prophylactic or curative treatment for ALS. The 2-amino-6-trifluoromethoxy-benzothiazole (Riluzole) (Mizoule et al., 1985) is the only approved disease-modifying agent that has been shown to prolong survival of ALS patients by a few months (Bensimon et al., 1994; Miller et al., 2003). Riluzole exerts its neuroprotective effects by blocking both voltage-gated sodium channels (Na^+) and N-methyl-D-aspartate (NMDA) receptors thereby preventing excessive calcium influx into neurons (Hubert et al., 1994; Malgouris et al., 1994).

1.1.2 Cellular and molecular mechanism underlying ALS

Cu/Zn superoxide dismutase mutation

First insights into the cellular and molecular basis of ALS began with the identification of mutations in the copper/zinc superoxide dismutase gene (Cu/Zn, SOD1) (Rosen et al., 1993), accountable for approximately 20% of familial cases and 5% of apparently sporadic ALS (see Kiernan et al., 2011). Wild-type SOD1 is an abundant homodimeric and cytosolic enzyme ubiquitously expressed. This polypeptide comprises 153 amino-acid and is responsible for the conversion of superoxide radicals, a by-product of mitochondrial respiration, into molecular oxygen and hydrogen peroxide, as follows;

$$2O_2^- + 2H^+ \xrightarrow{SOD1} H_2O_2 + O_2$$

Copper atom, which binds one of the monomers, plays the active role in the removal of superoxide whereas zinc atom, bound to the other monomer, confers structural stability to the enzyme. This two-step process prevents the generation of reactive oxygen species (ROS), and hence, reduces oxidative stress in cells (see Cozzolino et al., 2008; Dion et al., 2009).

Currently, more than 130 different SOD1 mutations have been reported to cause ALS. These mutations are distributed throughout all five exons of the gene and most of them are point mutations affecting either the active site or the structure (see Cozzolino et al., 2008; Dion et al., 2009). Since SOD1-knockout mice do not present neurodegeneration (Reaume et al., 1996) and many SOD1 variants show normal (Gurney et al., 1994; Wong et al., 1995) or no enzymatic activity (Ripps et al., 1995; Bruijn et al., 1997), those mutations are responsible for imparting an additional toxic function rather than inducing a reduction or loss of superoxide scavenging activity (see Dion et al., 2009).

Model for the evolution

ALS is considered a multifactorial disease, as it results from a complex interplay between multiple pathological mechanisms. Also, it is considered a multisystemic disease (Pramatarova et al., 2001; Gong et al., 2000), where damage within motor neurons is determinant for disease initiation whereas damage within non-neuronal cells drives disease progression and spread (Clement et al., 2003; Boillee et al., 2006).

Most of the current knowledge about cellular and molecular events taking place during disease progression (figure 1.1) has come from studies with multiple animal models. During the early phase of the disease, where there are no clinical signs, mutant SOD1 primarily acts within motor neurons causing the early retraction of motor axons from their synapses at the neuromuscular junction (Frey et al., 2000; Fischer et al., 2004; Pun et al., 2006). The mutant protein is also known to disrupt several cellular

machineries such as mitochondria (Dal Canto and Gurney 1994; Wong et al., 1995; Kong and Xu 1998), axonal transport (Wong et al., 1995; Zhang et al., 1997; Williamson and Cleveland 1999), endoplasmatic reticulum (Atkin et al., 2006) and proteasome (Urushitani et al., 2002; Kabashi et al., 2004).

During the symptomatic phase, there is a massive activation of microglia (Hall et al., 1998) and astrocytes (Schiffer et al., 1996; Hall et al., 1998) besides the continuing damage within motor neurons. Mutant SOD1 acts within these non-neuronal neighbors triggering a reduction in the levels of the glutamate transporter (EAAT2) (Bruijn et al., 1997, Howland et al., 2002), thereby promoting excitotoxicity in motor neurons, as well as a reduced secretion of trophic factors and/or release of toxic factors (Elliott 2001; Hensley et al., 2003). The build-up of damage within motor neurons, due to both intrinsic and extrinsic factors, ultimately triggers the activation of a caspase-depedent cell suicide program (Raoul et al., 2002; Wengenack et al., 2004). Consequently, denervation leads to the widespread muscle weakness and later to the progressive paralysis.

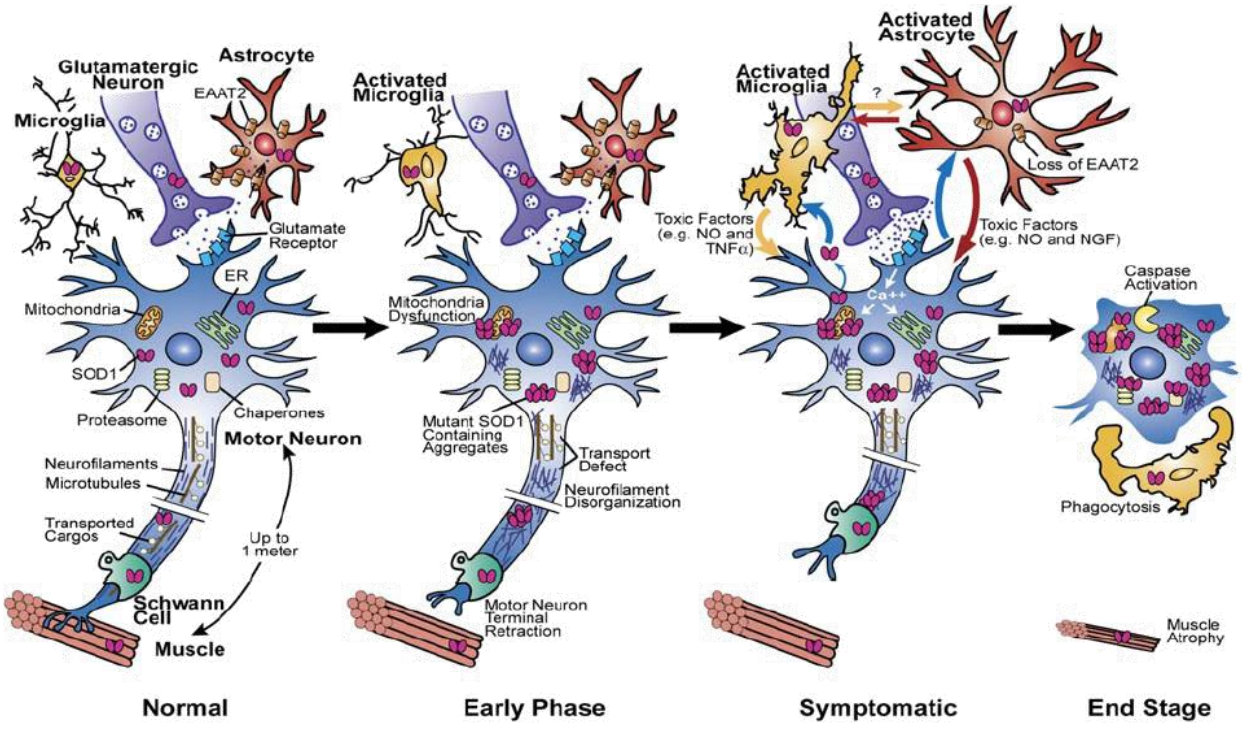

Figure 1.1 Model for the progression of ALS (from Boillee et al., 2006)

The early phase of the disease starts with the retraction of motor axons from their synapses. Aggregates containing missfolded SOD1 damage mitochondria, reducing ATP production and increasing free Ca^{2+} release, the endoplasmatic reticulum and the proteasome. Also, the disorganization of neurofilaments and/or mitochondrial defects lead to disruption of axonal transport. During symptomatic phase, mutant SOD1 triggers the inactivation of the glutamate transporter (EAAT2) in astrocytes, leading to an excessive influx of Ca^{2+} into lower motor neurons. In addition, activated microglia and astrocytes by reduced secretion of trophic factors or/and release of toxic factors into the cellular environment, amplify the initial damage and drive the progression of the disease. The end stage is characterized by paralysis and muscle atrophy with caspase-depedent cell death.

1.1.3 The dying-back and dying-forward hypothesis

At present, there is controversy whether disease starts distally, centrally or independently in upper motor neurons and lower motor neurons. The dying-forward hypothesis proposes that disease begins primarily in motor cortex, with upper motor neurons mediating in a latter phase the anterograde degeneration of lower motor neurons (by glutamate-induced excitotoxicity). The dying-back hypothesis, on the other hand, stands up for an initiation at the motor endplate, with a retrograde degeneration (see Kiernan et al., 2011).

Evidence for dying-back hypothesis

In the past decades, several studies that explored the spatio-temporal changes in motor neuron pathology in ALS (summarized in table 1.I) have been pointing to a retrograde degeneration. Both Frey and collaborators (2000) and Fisher and collaborators (2004) were the first groups to detect an early detachment of motor axons from their synapses at the neuromuscular junction in pre-symptomatic SOD1(G93A) mice, stating a dying-back axonopathy. Indeed, endplates denervation and motor axons loss were detected before soma degeneration and symptoms onset (Fischer et al., 2004), and fast-fatigable neuromuscular junctions presented a higher vulnerability to degeneration than slow-type synapses, thereby being lost early on (Frey et al., 2000).

The assessment of functional motor units loss in SOD1(G93A) mice by Hegedus and colleagues (2007; 2008) reinforced the dying-back hypothesis. These authors found a decline in motor unit numbers in fast-twitch muscles from day 40 and a concomitant decline in whole muscle contractile force. Later, they reported a preferential vulnerability of large motor units innervating IIB and IID/X fast-fatigable muscle fibers, together with a conversion to motor units innervating IIA fast-resistant muscle fibers.

More recently, a longitudinal MRI study performed by Marcuzzo and colleagues (2011) in the SOD1(G93A) mice revealed that muscle degeneration precedes neurodegeneration and clinical signs, supporting the retrograde dying-back of motor neurons.

Muscle as the primary site of degeneration

Besides the dying-back hypothesis, some studies suggest that skeletal muscle is the primary site of toxicity and the cause of the retraction of motor axons. Dupuis and colleagues (2002) demonstrated a shift in muscle gene expression, with an up-regulation of the neurite outgrowth inhibitor Nogo–A, in skeletal muscle from SOD1(G93A) mice and ALS patients. This suggests that muscle can play a key role in initiating

and modulating the disease, a finding consistent with the positive outcomes of treatments acting on muscle fibers, as IGF1 (Dobrowolny et al., 2005).

Moreover, it was detected that SOD1(G93A) mice suffer from a dramatic defect in energy homeostasis that seems to be linked to an abnormal hypermetabolism mainly of muscular origin (Dupuis et al., 2004). Consistent with this hypothesis, a mouse model of muscle restricted mitochondrial defect (similar to the hypermetabolism) is able *per se* to destabilize neuromuscular junctions and generate motor neuron degeneration (Dupuis et al., 2009).

Finally, Wong and colleagues (2010) showed that the restricted expression of the mutant SOD1 in muscle is sufficient to trigger motor neuron degeneration with a phenotype consistent with ALS.

1.2 The neuromuscular junction

The neuromuscular junction is the synapse between a spinal motor neuron and a skeletal muscle fiber. This system is responsible for transmitting the electric impulse from the nervous system to the muscle, triggering muscle contraction.

1.2.1 Structure of the neuromuscular junction

In mostly higher vertebrates, each skeletal muscle fiber is innervated at a single site by a single motor axon. As the motor neuron approaches the muscle fiber, the axon loses its myelin sheath and divides into fine branches. The ends of the branches form multiple expansions, called synaptic boutons, which make synaptic contacts with the muscle fibers membrane at a specialized region, the motor the endplate (Kandel, 2000).

Each nerve ending contains all the machinery required to release the neurotransmitter including synaptic vesicles, voltage-gated calcium channels (Ca^{2+}) and numerous mitochondria. Synaptic vesicles (also termed *quanta*) store acetylcholine (ACh) which is the only neurotransmitter at the skeletal neuromuscular junctions. ACh is first produced locally from acetyl coenzyme A (acetylCoA, synthesized from glucose) and choline (transported from the plasma) by choline acetyltransferase (ChAT) and then loaded into vesicles through vesicular transport (Purves, 2001). The number of ACh molecules inside a single vesicle, termed *quantum* of transmitter, varies from 500 to 10 000 (Kuffler and Yoshikami 1975) and was shown to vary with the functional state of the nerve terminal (Brooks and Thies, 1962; Naves and Van der Kloot, 2001).

Table 1.I. Major studies performed in SOD1 model of ALS and pointing for a dying-back pathology.

Aim	Observation	Major findings and conclusions
Quantification of lumbar spinal motor neurons and axons in nerve ventral roots (L-4), and the degree of denervation at NMJ (medial gastrocnemius (MG), tibialis anterior (TA) and soleus (SOL) muscles) in SOD1(G93A) and non-TG littermates. **Fisher et al. (2004) Experimental Neurology**	40% of denervation at the neuromuscular junction by day 47, followed by approximately 60% loss of motor axons from ventral roots between days 47 and 80, and loss of α-cell bodies from the lumbar spinal cord after day 80.	**Motor neuron pathology begins at the distal axon proceeding in a dying-back pattern.**
Recordings of both whole muscle and motor unit (MU) isometric contractile forces (MG, TA, extensor digitorumlongus (EDL) and SOL muscles)in SOD1(G93A) and SOD1(WT) mice. **Hegedus et al. (2007) Neurobiology of Disease**	Significant decline in the motor unit number in fast-twitch muscles (MG, TA and EDL muscles) by day 40 of age, which parallels reductions in whole muscle force. SOL muscle decline in both parameters was only apparent after symptoms onset.	**Denervation is prior to symptoms onset and proceeds in a muscle-specific manner: larger motor neurons innervating IIB and IID/X fibers, present increased susceptibility.**
Histological and Western blot analysis of SOL muscle in SOD1(G93A) and non-TG littermates **Narai et al. (2009) Neurology International**	Neurogenic atrophy of SOL muscle fibers and detachment of the nerve terminals from NMJ by 10 weeks of age. The levels and clusters of AChR did not change along the disease.	
Neurologic, histopathological and biochemical examination in transgenic mice with skeletal muscle-restricted expression of three different hSOD1 gene variants (hSOD1(G37R), hSOD1(G93A), hSOD1(WT)) **Wong and Martin (2010) Hum molec genet**	Transgenic mice with skeletal muscle-restricted expression of mSOD1develop neurologic and histopathologic phenotypes consistent with ALS. Muscle restricted expression is sufficient to cause dismantlement of NMJ and distal axonopathy.	**Muscle degeneration or injury can itself lead to neurodegeneration and cause ALS, rather than be a consequence of neurogenic atrophy.**
Longitudinal magnetic resonance imaging (MRI) of Hind limb muscle, brainstem and motor cortex of SOD1(G93A)(1Gur) and B6SJL control mice. **Marcuzzo et al. (2011) Experimental Neurology**	Significant reduction in muscle mass that parallels reduction in fiber diameter and muscle atrophy from week 8. Evidence of neurodegeneration in the brainstem detected only from week 10.	**Muscular degeneration precedes neurodegeneration and clinical signs. Secondary motor neurons are the first affected by this process.**

Synaptic vesicles can be attributed to three functionally different pools. The readily releasable pool comprises synaptic vesicles clustered at active zones, the specialized region for transmitter vesicular release, and sustains low and moderate neurotransmission. The cycling pool, located near the active zones, ensures the replenishment of the readily releasable pool. Recycled synaptic vesicles can either incorporate the readily releasable or the cycling pool. Finally, the reserve pool, located further away, sustains the replenishment of the below pools and is recruited only upon long-term transmission (Richards et al., 2003, see Rizzoli and Betz 2005).

The space between the nerve and muscle fibers is termed the synaptic cleft and consists in a condensed extracellular matrix (basement membrane or basal lamina) composed of collagen and glycoproteins with a structural function in organizing the synapse. Both the nerve and muscle fibers secrete proteins into the basement membrane namely acetylcholinesterase (AChE). This is a high catalytic enzyme that, by cleaving ACh into acetate and choline, limits both temporal and spatial extent of transmitter action (Kandel et al., 2000).

The motor endplate is characterized by a deep folding of the sarcolema. The crests contain a high density of ACh receptors, whereas the depths present a high density of voltage-gated sodium channels (Na^+). Post-synaptic actions of ACh are mediated by the ionotropic nicotinic ACh receptors, which are non selective cation channels (Kandel et al., 2000).

1.2.2 Neuromuscular transmission

Most of the knowledge on synaptic transmission comes from the pioneering work on neuromuscular transmission performed by Bernard Katz and his colleagues during the 1950s and 1960s.

Resting membrane potential

The resting membrane potential (RMP) is the electrical potential measured across the cell membrane in the absence of signaling. It results from a separation of charges that, in general terms, is due to differences 1) in the concentrations of specific ions across cell membrane and 2) in the selective permeability of the membrane to some of these ions. The negative membrane potential indicates an excess in negative charges within the cell, and can be predicted by the Goldman equation;

$$RMP = \frac{RT}{F} \ln \frac{P_K[K^+]_o + P_{Na}[Na^+]_o + P_{Cl}[Cl^-]_i}{P_K[K^+]_i + P_{Na}[Na^+]_i + P_{Cl}[Cl^-]_o}$$

Where R indicates the gas constant, T the temperature, F the faraday constant, P the permeability of the membrane for the ion X, and $[X]_o$ and $[X]_i$ the concentrations of the ion inside and outside the muscle fiber. In these conditions, cells are in a steady state with no net flux of ions across the membrane.

During synaptic transmission, the temporary opening of ion channels produces brief changes in the flow of electrical current across the cell membrane that drives the membrane potential away from its resting value (Purves, 2001; Kandel et al., 2000).

Evoked activity

During nerve stimulation, the action potential propagating along the axon reaches the nerve terminal and the resulting depolarization causes the opening of voltage-gated Ca^{2+} channels. The subsequent influx of Ca^{2+} raises the intracellular free Ca^{2+} concentration in the pre-synaptic terminal triggering the synchronous fusion of the synaptic vesicles with the pre-synaptic membrane. The number of quanta released by each nerve impulse is known as *quantal content* of the EPP.

In the post-synaptic membrane, the activation of nicotinic ACh receptors by two molecules of ACh increases the total conductance of the endplate membrane, allowing Na^+ and K^+ to flow with nearly equal permeability. This local depolarization, called the endplate potential (EPP), is normally large enough to bring the membrane potential of the muscle fiber above the threshold for the activation of voltage-gated Na^+ channel. By a positive feedback loop, more voltage-gated Na^+ channels are activated, producing an actively propagated action potential that ultimately triggers muscle contraction (Purves, 2001; Kandel et al., 2000).

Spontaneous activity

In the absence of nerve stimulation, spontaneous deflections of the resting membrane potential are also detected (Fatt and Katz 1952). These small depolarizations (<1 mV) are designated miniature endplate potentials (MEPPs) and arise from the spontaneous asynchronous release of individual vesicles. “Giant” miniature endplate potentials (GMEPPs) (Liley 1957) are classified separately from the usual MEPPs. These arise from a spontaneous synchronous release of multiple vesicles insensitive to both nerve terminal depolarization and extracellular Ca^{2+} (Colmeus et al., 1982; Thesleff et al., 1983) being instead triggered by Ca^{2+} released from intracellular stores and/or result from an impaired processing of recycled vesicles (Rizzoli and Betz 2002). Moreover several studies reported an increased frequency of GMEPPs in re-innervated muscles (Miledi 1960), nerve terminals in degeneration (Birks et al., 1960) and in motor endplate diseases (Weinstein 1980).

Safety factor

The transmission of signals from nerve to skeletal muscle is a highly reliable process that is necessary for the normal function of the body. Motor nerve terminals release more *quanta* per nerve impulse than the required to initiate an action potential. This excess is referred as safety factor and allows the neuromuscular transmission to remain effective under several physiological conditions and stresses. Numerous diseases characterized by an impairment of neuromuscular transmission, and therefore by a weakness of voluntary contraction, present a reduced safety factor (see Wood and Slater 2001).

1.3 ALS and the neuromuscular junction

1.3.1 Molecular changes

Mitochondria and axonal transport are considered key players in many cellular processes relevant for neuromuscular transmission and their impairment, as reported in ALS, might be related to changes in neuromuscular junction function.

Mitochondria are vital organelles with a predominant role in energy metabolism providing ATP for axonal transport, ion pump fueling (Na^+/K^+), neurotransmitter synthesis, and for several steps in the vesicle cycle such as vesicle fusion, uncoating and refilling. This metabolite is also essential to sustain neurotransmission during high-frequency stimulation mediating the mobilization of vesicles from the reserve pool and recycling via endocytosis. Mitochondria are specifically retained in regions of the axon with high energy-demand including Ranvier nodes and nerve terminals in particular near the actives zones (Vos et al., 2010 and Kawamata and Manfredi 2010). In ALS, mutant SOD1 was reported to accumulate in vacuoles in the mitochondrial intermembrane space (Higgins et al., 2003). In accordance, defects in the mitochondrial respiratory chain (ATP-generating oxidative phosphorylation) were observed in both ALS patients tissues (Wiedemann et al., 2002) and transgenic mice (Mattiazzi et al., 2002). Moreover, mutant SOD1 was also reported to disrupt anterograde transport of mitochondria, inducing an accumulation of mitochondria in cell bodies and in proximal axons of transgenic mice (De Vos et al., 2007). Consistent with this, the reduced mitochondrial content in the distal axon combined with the impaired mitochondrial function may lead to a local ATP depletion, thereby inducing axonal stress and compromising neuromuscular transmission (De Vos et al., 2007).

Mitochondria also contribute to neuronal function through regulation of calcium homeostasis. This organelle is able to sequester and release Ca^{2+} and thereby modulates numerous events such as the probability of neurotransmitter release (promoting either recovery from depression or vesicles depletion),

and the endocytic rate within vesicle recycling process (see Vos et al., 2010; Kawamata and Manfredi 2010). In ALS, motor nerve terminals present a lower cytosolic calcium clearance (Vila et al., 2003; Jaiswal et al., 2009; Nguyen et al., 2009) and muscle fibers present both reduced mitochondrial Ca^{2+} uptake and increased Ca^{2+} release from endoplasmatic reticulum stores (Zhou et al., 2010). This reduction in calcium buffering leads to an increase in intracellular calcium levels making motor neurons more vulnerable to degeneration (Siklos et al., 1998; Kim et al., 2002).

Finally, mitochondria constitute an important source of reactive oxygen species (ROS) through mitochondrial respiration (Vos et al., 2010 and Kawamata and Manfredi 2010). Hydrogen peroxide (H_2O_2), which is generated from the superoxide by SOD1, was reported to be a modulator of transmitter release. While low physiological concentrations of H_2O_2 were shown to facilitate neuromuscular transmission by enhancing transmitter release (Giniatullin and Giniatullin 2003), high concentrations caused synaptic depression through a direct impairment of the releasing machinery, mediated by SNAP25 essential fusion protein (Giniatullin and Giniatullin 2003, Giniatullin et al., 2006). In ALS, multiple pathological studies have reported evidence of increased oxidative stress in postmortem tissue from patients (Shaw et al., 1995; Simpson et al., 2004).

Motor neurons are polarized and contain long processes, often with more than a meter in length, through which cargoes have to move. Axonal transport is therefore a key component in structure maintenance and signal transmission, namely neurotransmitter synthesis, release and recycling, at the nerve terminals of motor axons. In ALS, mutant SOD1 species were shown to bind KAP3, a component of the kinesin-2 motor complex that mediates the transport of ChAT. Consistent with this, both ChAT levels at nerve terminals and ACh release, were reduced (Tateno et al., 2009).

1.3.2 Functional changes

Figure 1.2 illustrates the current knowledge on neuromuscular transmission in ALS. At present, there is little information regarding pre-symptomatic phase. Souayah and colleagues (2012) reported that 6 weeks-old SOD1(G93A) mice presented a reduced probability of successful neuromuscular transmission (more failures) at high frequencies of stimulation (70 and 90 Hz). This functionally compromised phenotype was attributed by the authors to an impaired action potential initiation and propagation along the axon or impairments in transmitter mobilization and release from the nerve ending.

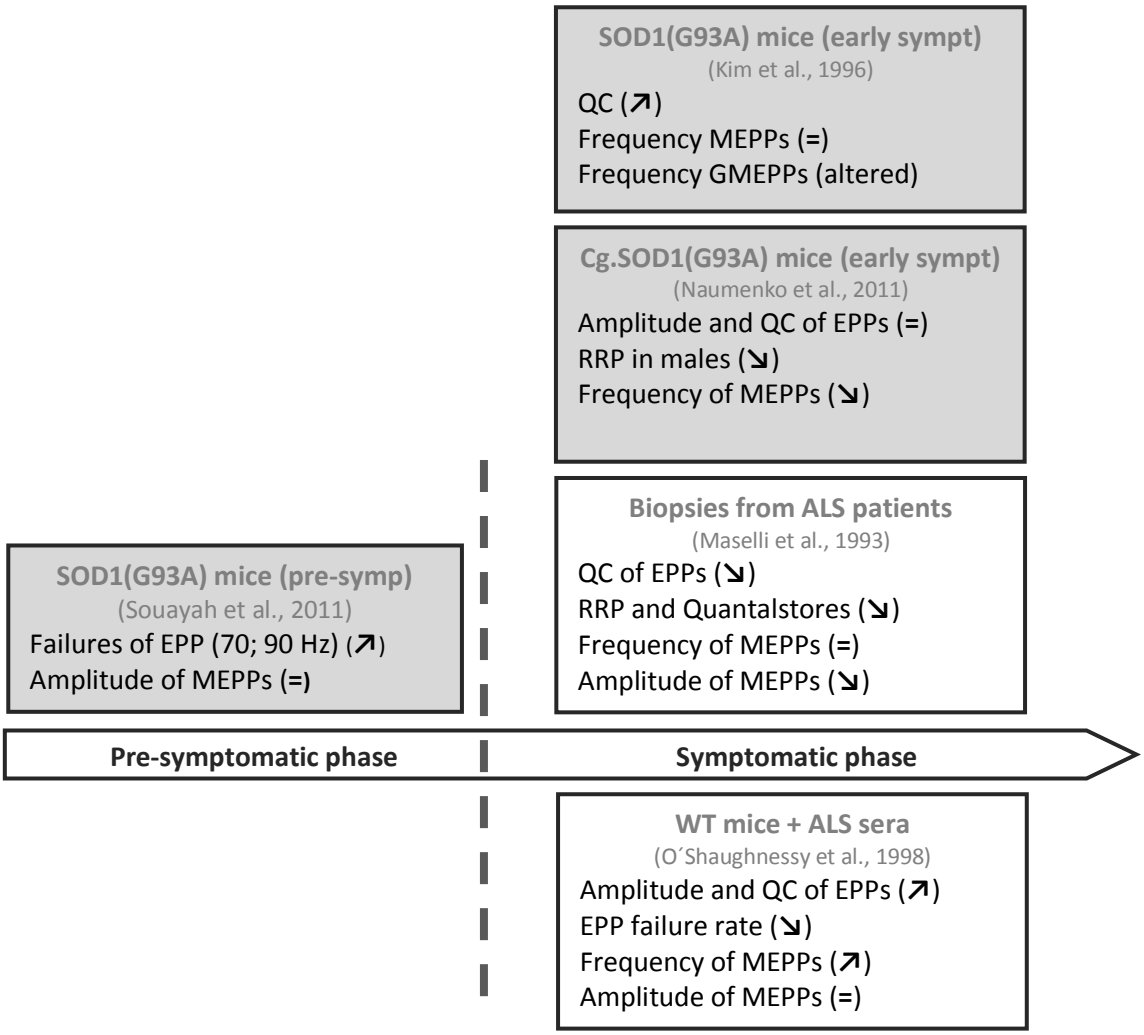

Figure 1.2 Current knowledge on neuromuscular transmission in ALS

Here is summarized the results from major electrophysiological studies in both pre-symptomatic and symptomatic phases of ALS disease. Grey boxes show studies performed in mice models of ALS whereas white boxes show studies performed with samples from ALS patients. In pre-symptomatic phase, Souayah and colleagues (2012) assessed neuromuscular transmission of 6weeks-old SOD1(G93A). In symptomatic phase, Kim (1996) and Naumenko (2011) groups looked at neuromuscular transmission of SOD1(G93A) and congenic SOD1(G93A) mice respectively, when both models started to show signs of disease. Electrophysiological recordings in anconeus muscle biopsies from ALS patients (Maselli et al., 1993) or in WT mice passively transferred with sera from sporadic ALS patients (O'Shaughnessy et al., 1998) were also studied. ↗indicates an increase↘,a decrease and =no changes when compared to the control. QC, *quantal content*; EPP, endplate potential; MEPPs, miniature endplate potentials; RRP, readily releasable pool.

Regarding symptomatic phase, contradictory results were published. Maselli and colleagues (1993) reported that anconeus muscle biopsies taken from ALS patients presented an impaired neuromuscular transmission with a reduced mean *quantal content* of EPPs, mean quanta available for immediate release, as well as mean quantal stores. Whereas the mean frequency of MEPPs remained unchanged, the mean amplitude of MEPPs was similarly decreased. Naumenko and colleagues (2011) however did not observed

differences in the amplitude and *quantal content* of EPPs in symptomatic congenic SOD1(G93A) transgenic mice. Whereas there was a dramatic drop in spontaneous activity with a reduced mean frequency of MEPPs, no alterations in the amplitude of MEPPs were detected. Male neuromuscular junctions were also reported to present a reduced readily releasable pool and to be more vulnerable to reactive oxygen species. In contrast, a preliminary study performed by Kim and colleagues (1996) detected an increased mean *quantal content* in symptomatic SOD1(G93A) mice (10-12 weeks-old) and no changes in both frequency and amplitude of MEPPs. Although no details were provided by the authors, the frequency of GMEPPs was reported to be changed.

Interestingly, the passive transfer of sera from sporadic ALS patients to wild-type mice increased the evoked transmitter release (amplitude and mean *quantal content*) and spontaneous activity (frequency of MEPPs) (O'Shaughnessy et al., 1998). In accordance, either passive transfer or pre-incubation of neuromuscular junctions with immunoglobulins G (IgGs) from ALS patients had already been reported to increase the frequency of MEPPs (Uchitel et al., 1988; Uchitel et al., 1992). Consistent with this, Pagani and colleagues (2006) showed that IgGs from ALS patients interacted with nerve terminals potentiating spontaneous release through the activation of both N-type ($Ca_V2.2$) channels and IP_3 receptors, and Gonzalez and colleagues (2011), through P/Q-type ($Ca_V2.1$) channels.

2 Goals

ALS is the most frequent adult-onset motor neuron disease. Currently, numerous authors have been pointing for a dying-back disease. Since the neuromuscular junction might be the first site to be affected and, therefore, where first signs of the disease can be detected at early stages, there is a need to focus on neuromuscular junction parameters.

At present there is little information about neuromuscular transmission in the SOD1(G93A) mice, and the existing one is often controversial. We considered therefore of interest to evaluate neuromuscular function with the following specific goals:

1. To investigate if the evoked and spontaneous neuromuscular transmission is impaired in pre-symptomatic phase of the disease,
2. To investigate if the evoked and spontaneous neuromuscular transmission is impaired in symptomatic phase of the disease,
3. To investigate if symptomatic transgenic mice present differences in evoked and spontaneous neuromuscular transmission when compared to pre-symptomatic transgenic mice.

To meet the previous aims we performed the following tasks:

1. Establishment and maintenance of the SOD1(G93A) colony at IMM facilities,
2. Litters genotyping in order to distinguish transgenic from non-transgenic mice,
3. Behavioral phenotyping to evaluate motor function and validate therefore the phase of the disease.
4. Intracellular recordings in phrenic-nerve diaphragm preparations from transgenic and non-transgenic mice in two age groups: 4-6 and 12-14 weeks-old corresponding respectively to pre-symptomatic and symptomatic phases of ALS.

3 Materials and methods

3.1 Animals

3.1.1 Animal model

Animal models are of extreme importance since they constitute a major tool to explore the etiology and pathogenesis of diseases and to test possible therapeutic approaches. In the framework of ALS, as most human samples are obtained from patients at the terminal stage, the investigation of pathogenic mechanisms operating from disease onset to death becomes nearly impossible without resorting animal models (see Kato 2008).

Table 3.I. Characteristics of main mutant SOD1 mouse models (adapted from Swarup and Julien 2011)

SOD1 mutant (Reference)	Inheritance	Enzyme Activity	Protein stability	Disease onset	Disease Progression
G93A (Gurney et al. (1994) Science)	Dominant	Active (11 fold)	Stable	Early (3-4 mo)	Moderate (3 wks)
G86R (Bruijn et al. (1997) Neuron)	Dominant	Inactive (0 fold)	Reduced	Late (7,5mo)	Fast (2wks)
G37R (Wong et al. (1995) Neuron)	Dominant	Active (14.5 fold)	Reduced	Moderate (4-6 mo)	Slow (4-6 wks)

The generation of ALS animal models started after the identification of *sod1* as a causative gene for this disease (Rosen et al., 1993). Until now more than 12 transgenic mice carrying different SOD1 mutations have been created by inducing the expression of mutant *sod1* mini-genes. These are constructs involving typically 12-15kb human genomic fragments, encoding mutated SOD1, driven by endogenous promoter and regulatory sequences (see Turner and Talbot 2008). Table 3.I presents the characteristics of major SOD1 transgenic lines. As illustrated, these lines differ in transgene copy number, enzyme levels and activity, as well as disease onset and progression. Despite the vast differences, all of them have been reported to exhibit the same histopathological hallmarks that are observed clinically in both sporadic and familial ALS (see Julien and Kriz 2006). More importantly, mice that express wild-type human SOD1 do not develop this stereotyped syndrome suggestive of motor neuron disease (Gurney et al., 1994). More recently, the discovery of other genes implicated in ALS namely alsin, dynactin, senataxin, VAPB, FUS and

TDP-43, has lead to the creation of new animal models. Nevertheless, SOD1 models remain the only reliable mouse model for either sporadic or familial ALS (see Swarup and Julien 2011).

In the present study we used the SOD1(G93A) model (Gurney et al., 1994) since it constitutes the most widely used and the best-characterized mouse model of ALS, as illustrated in figure 3.1. These animals carry a high copy number (25±1.5) of the human SOD1 gene (transgene) with a point mutation responsible for a glycine to alanine substitution at position 93.

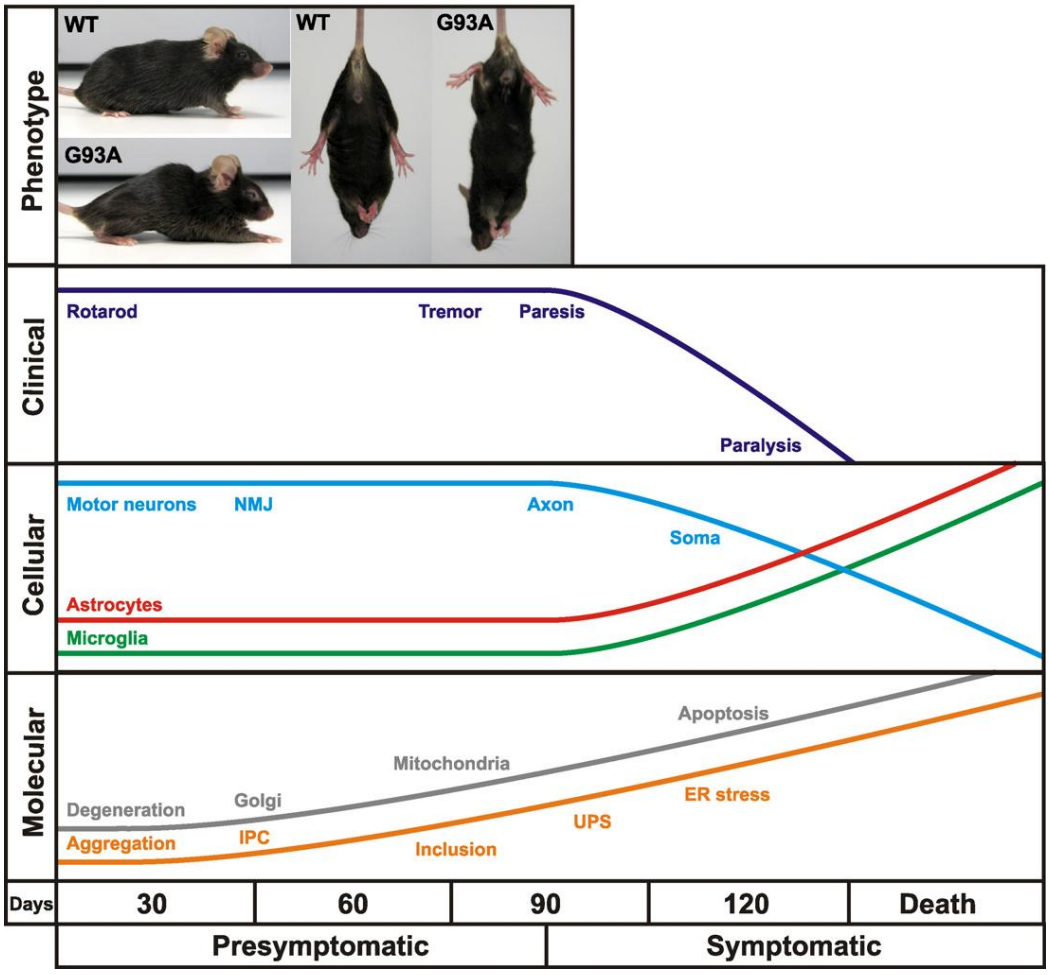

Figure 3.1 Time course of clinical and neuropathological events in SOD1(G93A) mice (from Turner and Talbot 2008)

Clinically, mice begin to show signs of hind limb tremor and weakness by 3 months of age. From 3 to 4 months, mice progress to hyper-reflexia, paralysis and premature death. At the cellular level, neurodegeneration begins with denervation of neuromuscular junctions, followed by a significant axonal loss and soma loss. A massive activation of astrocytes and microglia becomes visible at approximately disease onset. Finally, at the molecular level, pathologic features of motor neurons include mitochondrial vacuolization, Golgi apparatus fragmentation, neurofilament-positive inclusions, mutant SOD1 aggregation into insoluble protein complexes (IPC) (Turner and Talbot 2008).

3.1.2 Animal strains, breeding and husbandry

Transgenic B6SJL-TgN(SOD1-G93A)1Gur/J males (Jackson Laboratory, No. 002726) and wild-type B6SJLF1/J females were purchased from Jackson Laboratory (USA) and a colony was established at BEEM facilities. Since transgenic females are infertile, mice were maintained on a background B6SJL by breeding transgenic males with non-transgenic females in a rotational scheme.

At time of weaning, littermates were identified through ear punching and separated in different cages according to their gender. This system is a permanent procedure that attributes to each hole a number and so allows individual identification of mice. Moreover, this method does not require anesthesia, guarantee animal welfare, and the tissue removed by the ear punch can be used for DNA analysis, phasing out the requirement of an additional procedure. All animals were housed 4-5 mice/cage, under a 12h light/12h dark cycle, and received food and water *ad libitum*. Animals were handled according to European Community guidelines and Portuguese Law on Animal Care.

3.2 Genotyping

A polymerase chain reaction (PCR) was then conducted to differentiate between non-transgenic and transgenic mice. Ear tissue punches taken from each mice were placed separately in microcentrifuge tubes along with 0.1ml of DNA digestion buffer (50mM KCl, 10nM Tris-HCl (pH 9.0) and 0.1% Triton X-100 with proteinase K added to a final concentration of 0.15 mg/ml) and were incubated overnight at 56ºC. A gentle shaking was applied in order to aid complete tissue disruption. After incubation, proteinase K was inactivated by placing tubes in a dry heating block set at 95ºC for 15min. Samples were then centrifuged for 2 min at 1200rpm to get rid of debris and supernatants were transferred into new autoclaved eppendorfs tubes. DNA samples were either used immediately as templates for amplification reaction or stored at -20ºC.

Table 3.II. Protocol Primers (adapted from Jackson´s Laboratories manual)

Primer	Sequence 5' --> 3'	Primer Type
oIMR0113	CAT CAG CCC TAA TCC ATC TGA	SOD1 Transgene
oIMR0114	CGC GAC TAA CAA TCA AAG TGA	SOD1 Transgene
oIMR7338	CTA GGC CAC AGA ATT GAA AGA TCT	Internal Positive Control Forward
oIMR7339	GTA GGT GGA AAT TCT AGC ATC ATC C	Internal Positive Control Forward

A mix solution was prepared (15.7µl H_2O autoclaved, 2.50µl 10xPCR Buffer II, 2.5mM of each dNTPs, 20µM of each primer (presented on table 3.II) and 5U/µl Taq DNA polymerase, to a final volume of 25µl/sample), taking into account the number of DNA samples and controls to run, plus 10% extra for losses while pipeting. IMR0113 and IMR0114 amplify SOD1 human fragment while IMR7338 and IMR339 amplify a internal positive fragment. After pipeting 25µl of the mix reaction into PCR tubes, 1µl of each DNA sample was added, and tubes were placed in a termocycler device for PCR assay. After an initial denaturation step of 3min at 94ºC, DNA was amplified for 29 cycles (30s at 94ºC, 30s at 62ºC and 30s at 72ºC) followed by a final elongation step of 10 min a 72ºC and a cool down step, where solutions are maintained at 4ºC.

Finally, PCR products were separated on a 2% agarose gel. To do that, 5µl of loading buffer was added to each sample tube, and then 15µl of the mixture was loaded to the gel-well. To allow band size estimation, 6µl of the BenchTop 100bp DNA ladder was also applied. Gel was run for 30 to 40min at 100 volts in an electrophoresis bath containing 1x Tris-Acetate-EDTA (TAE) buffer and then placed under UV light for band inspection. Figure 3.2 shows an example of a progeny genotyping with the SOD1 and WT bands on the agarose gel. Wild-type mice present a unique band of 324pb corresponding to the internal positive control, while transgenic mice exhibits 2 bands, the 236pb and 324bp corresponding to the transgene and internal positive standard respectively.

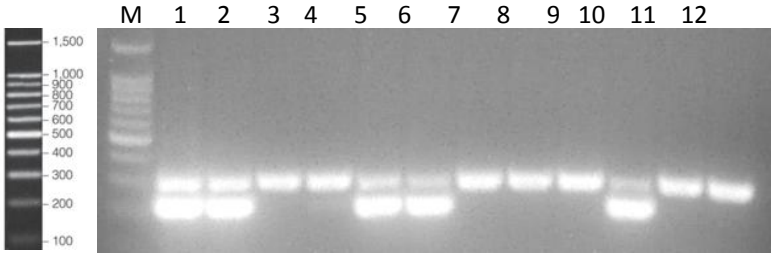

Figure 3.2 Example of a progeny genotyping
Here is illustrated the identification of SOD1 and WT mice on a 2% agarose gel. On the left side is the BenchTop 100bp DNA ladder separated equally on a 2% agarose gel. The PCR product of the WT genotype (lane 11) is a fragment of 324bp whereas the one of SOD1 mice (lane 5) are two fragments of 236 and 324bp. Lane under M in the gel is the 100bp size marker.

3.3 Behavioural phenotyping

3.3.1 Body weight

Body weight is easy to measure and can be indicative of general wealth of mice. However, the correlation between the process of weight loss and changes in locomotor coordination and muscular strength is difficult (Knippenberg et al., 2010). In this way body weight was recorded has an additional parameter.

3.3.2 Rotarod test

At present, rotarod is considered the gold standard test to assess motor function in mice (see Brooks and Dunnett 2009). As shown by Knippenberg and colleagues (2010), is the most sensitive and appropriate method for early detection of symptoms onset in the SOD1(G93A) mouse model. The rotarod apparatus is illustrated in figure 3.3. Briefly, mice are placed on the rotating rod where they have to maintain their balance and motor coordination to remain on it. When mice fall from the rod, sensing platforms (a trip switch on the floor below) stop the counter and latency-to-fall is recorded. This test can be performed at fixed or accelerating speeds. Fixed-speed test are known to provide separate data on each range and does not confound motor coordination with fatigue as the accelerating test do. In addition, this version was reported to be more appropriate to detect small changes with a maximum sensitivity (Monville et al., 2006; Brooks and Dunnett 2009)

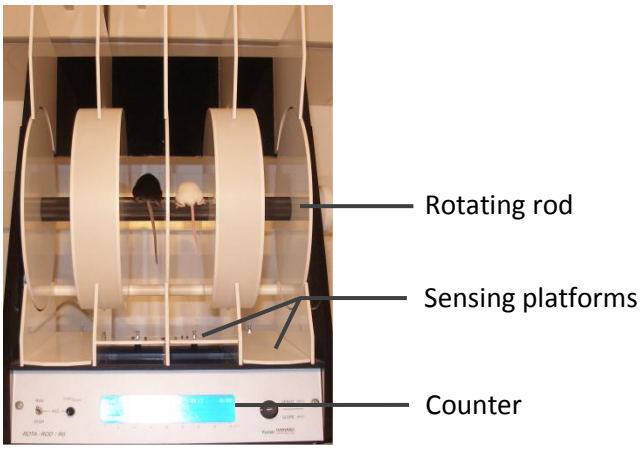

Figure 3.3 Rotarod device
Mice falling from the rotating rod push the platforms. This stops the counter and in this way the latency-to-fall is recorded.

In the context of ALS, multiple rotarod protocols have been generated. Most of them were used to assess disease onset and progression while testing new drug treatments and so where performed in an overtime fashion. Typically, fixed speed tests are performed at 10 or 15 rpm with a cut-off time set at 180s (Smittkamp et al., 2008; Banerjee et al., 2008) and accelerating versions increase speed from 2 to 20 rpm over the course of 300s (Smittkamp et al., 2008) or 1 to 18 rpm during 180s (Knippenberg et al., 2010).

In the present study rotarod was conducted in two age groups: in animals with 4-6 and 12-14 weeks. A training period comprising two stages was performed so as to minimize environmental variability. First animals were habituated to handling, initiated four days before the testing day, then to the rotarod apparatus and finally were taught the task itself. For that, mice were placed on the rod at the lowest rotation speed (4 rpm) where they had to maintain for at least 120s. Once the task was learnt, mice were placed and taken off from the rod several times by the researcher in order to reduce handling stress (Rozas et al., 1997). In the testing day, mice were sequentially assessed at 5, 10, 15, and 25 rpm, for a maximum of 300s each speed. 3 trials were performed per speed with 5 min rest between each trial.

3.4 Electrophysiological recordings

3.4.1 The neuromuscular junction model

Since the turn of the century, the neuromuscular junction of vertebrate skeletal muscle has served as a model for studying synaptic transmission conveying most of our current knowledge about neurotransmission within central and peripheral nervous system.

This synapse has been considered a prototype model due to its accessibility (located at periphery), size, and more importantly its simplicity, facilitating the experimental analysis (Deschenes et al., 1994). Indeed, each muscle fiber is innervated by a single motor neuron, so any event occurring in this cell results from just one input. This is not the case in central nervous system where one neuron can receive a thousand of different inputs, either excitatory or inhibitory, from adjacent neurons. Additionally, the only input is excitatory and results from the action of ACh. This neurotransmitter is released in multimolecular packets or *quanta*, and the number of *quanta* release by an EPP, that is the *quantal content*, can be easily assessed. Finally, since the amplitude of any synaptic potential depends upon both the amount of transmitter released and the postsynaptic responsiveness to transmitter, the differentiation between pre and post-synaptic factors becomes possible. Typically changes in MEPPs frequency are related to the pre-synaptic component. Changes of MEPPs amplitude may reflect both pre- and postsynaptic factors. Generally it results from changes in post-synaptic action of ACh or changes in postsynaptic membrane

resistance or capacitance. If these remain unchanged, then this difference has a pre-synaptic origin, such as less ACh contained in each *quanta*. Additionally, the electrophysiological assessment provides an excellent time resolution of events and the method is relatively simple. It constitutes the best way to evaluate the nerve-muscle communication and hence to detect impairments (Naguib et al., 2002).

3.4.2 Diaphragm phrenic-nerve preparation

Experiments were conducted in animals with 4-6 and 12-14 weeks-old. Non-transgenic littermates (WT) were used as age-matched controls. At the different stages of disease, mice were anesthetized with gaseous isoflurane and then sacrified by decapitation. Hemi-diaphragm muscle with its attached phrenic-nerve was isolated and then mounted on a 3ml Perspex chamber in order to be maintained at resting tension as illustrated in figure 3.4. Tissue was perfused continuously with a gassed (95% O_2 and 5% CO_2) physiological saline solution (containing (mM): NaCl 117; KCl 5; $NaHCO_3$ 25; NaH_2PO_4 1,2; glucose 11; $CaCl_2$ 2,5; $MgCl_2$ 1,2) kept at room temperature (22-25ºC). Perfusion was maintained at a rate of 3ml/min *via* a roller pump, and bath volume was kept constant by suction.

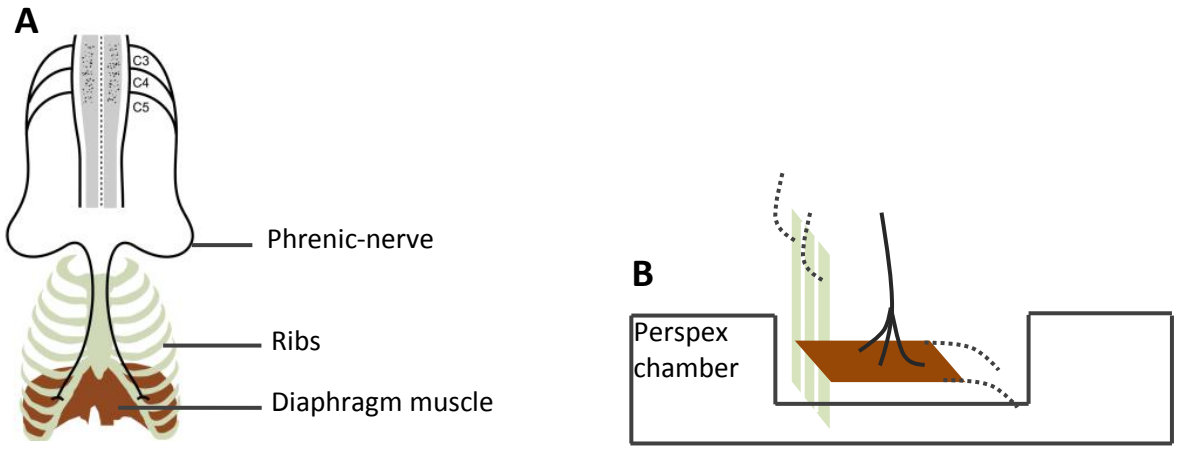

Figure 3.4 Scheme depicting diaphragm phrenic-nerve preparation
A) Phrenic motor neurons together with a strip of the innervated diaphragm muscle and ribs are isolated (adapted from Mantilla and Sieck 2009) and then B) assembled in a perspex chamber to be maintained at resting tension.

3.4.3 Muscle contraction blockade

Before any recording, muscle action potential had to be blocked in order to prevent mechanical disturbance resulting from muscle contraction. This can be achieved by 1) raising [Mg^{2+}] or lowering [Ca^{2+}], 2) treating preparations with d-tubocurarine, or 3) damaging muscle fibers. In the framework of this study, however, these alternative approaches present the limitation that they do not allow the full effect of nerve activity to be measured. By contrast, the use of μ-conotoxin GIIIB, a natural toxin isolated from the venom of the snail *Conusgeographus*, allows EPP recording from intact muscle fibers without affecting *quantal content* of EPPs. This inhibitory peptide preferentially blocks muscle Na^+ channels and not those present on nerves (Cruz et al., 1985). In this study, muscle contraction was prevented by treating preparations with 2μM μ-conotoxin GIIIB for 45 to 60min, as done previously (Gillingwater et al., 2002). For this purpose, perfusion was stopped and toxin was applied to the solution bath, just beneath tissue preparation. During time treatment, preparation was kept under oxygenation. At the end, perfusion was retaken by turning on the roller pump. This procedure was repeated whenever contraction became visible.

3.4.4 Intracellular recordings

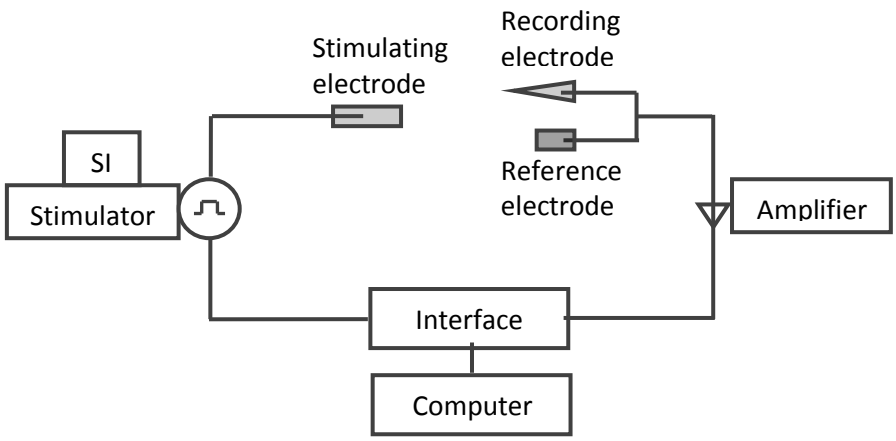

Figure 3.5. Diagram of the electrophysiological setup
The interface board first converts digital signals into analog allowing the computer to send command signals (stimulus duration, frequency, strength) to stimulate the nerve. Then, the current is delivered from the stimulator through the stimulus isolator (SI) and a suction electrode is use to stimulate the motor axons into firing action potentials. The resting membrane potentials (through channel 1) and spontaneous or evoked activity (through channel 2) are recorded simultaneously by the microelectrode and then sent into the amplifier through corresponding channels. Once amplified, the electrical (analogue) signals travel to the interface board to be converted into digital forms and then acquired by the computer using specially designed software.

Data acquisition

Intracellular recordings were performed in the conventional way (figure 3.5) (Ribeiro and Walker 1975; Ribeiro and Sebastiao 1987; Pousinha et al., 2012). Glass microelectrodes (10-30mΩ) filled with 3KCl were inserted within muscle fibers at the motor endplate and the reference electrode was an Ag-AgCl pellet placed in the bath.

For EPP recordings, the phrenic-nerve was stimulated supramaximally at 0.5 Hz, with constant current of 20 μs duration, by means of a suction electrode. It is known that quantal release, which is itself frequency dependent, gradually declines in response to stimulation frequencies greater than 1 Hz. Hence, the frequency of stimulation chosen ensured the measurement of individual responses to evoked activity without summation of postsynaptic potentials over time.

MEPPs were acquired in gap free mode during 100s. Through all the experiment, resting membrane potential (RMP) of the muscle fiber was monitored.

After recording, signals were amplified, digitalized and stored on a computer with Clampex program (pClamp10 Axon Instruments, Foster City, USA), to offline analysis of data.

Data offline analysis

The neuromuscular junctions considered for analysis had to meet 2 conditions: a stable resting membrane potential ranging from -50mV to -80mV and recordings in gap free mode with a basal noise lower than 0.3mV.

The evoked activity was measured during intervals of 10 minutes. The EPP amplitude represents the amplitude of 60 consecutive sweeps. As the magnitude of the recorded EPP is influenced by capacitive properties of the muscle fiber membrane (see Wood and Slater 2001) amplitudes were normalized to a membrane potential of -75 mV, as done previously (Sons and Plomp 2006; Pardo et al., 2006; Rozas et al., 2011) using the following equation;

$$V_{NOR} = [V_{OBS} \times (-75)] / RMP$$

V_{NOR} indicates the corrected amplitude, V_{OBS} the recorded amplitude and RMP the recorded resting membrane potential. This normalization allows the correction of the EPP amplitude from subtle changes in the resting membrane potential and/or subsequent comparisons of EPP amplitudes from neuromuscular junctions with different membrane potentials. Then, the mean amplitude of EPPs was calculated for each neuromuscular junction by averaging the 5 normalized EPP amplitudes. The *quantal content* of the EPPs, which indicates the number of vesicles released per impulse, was estimated through the indirect method as follows;

$$\text{mean QC} = \text{mean EPP}_{NOR} / \text{mean MEPP}_{NOR}$$

The mean EPP_{NOR} indicates the average evoked response normalized, and mean $MEPP_{NOR}$, the average spontaneous response normalized, both acquired during the same period.

Spontaneous events acquired during the time interval of 100s were detected by a detection protocol after application of a lowpass filter to attenuate high frequency noise. The threshold for MEPPs detection was set at levels between 0.2mV and 1mV of amplitude. This maximum amplitude was established in order to treat GMEPPs separately. Additionally, a minimum and maximum of events duration of 2 and 8 ms respectively were set in order to prevent signal contamination with electric noise. The mean amplitude of MEPPs was calculated by averaging the amplitude of each MEPP recorded. The same procedure was done to assess the mean rise-time of MEPPs and mean decay-time of MEPPs. Additionally the mean frequency of MEPPs was measured by counting the number of events acquired during the 100s. The minimum amplitude for GMEPPs detection was set at 1mV. The mean frequency of GMEPPs was calculated by counting the number of these events acquired during the 100s.

3.5 Statistical analysis

All data are presented as mean ± standard error mean (SEM) in each group, with n corresponding to the number of animals used or the number of neuromuscular junctions sampled, as indicated in each figure or table.

Statistical significance of differences between means was determined through GraphPad software. The parametric Student´s t test was used whenever both groups presented a normal distribution and equality of variances. Normality was tested through Shapiro-Wilk test (S-W), which is more appropriate for small samples ($n<30$), and homogeneity of variances tested through F test. Alternatively, the non parametric Mann-Whitney U-test (M-W) was applied when one of the groups was non-normally distributed, and Student´s t test with Welsh correction, when the equality of variances condition was not met (F test $p<0.05$).

The frequency distribution of MEPPs amplitude plotted the amplitude of all MEPPs recorded at WT and SOD1 neuromuscular junctions. Histograms with a bin width of 0.1mV ranged from 0.2mV to 1mV. Then a non-linear regression that better fit the distribution of data was added, being used a Gaussian distribution and a Sum of two Gaussians distributions. To evaluate if the model chosen best fitted the distribution we looked at R^2, which is a measure of goodness of fit. This ratio ranges between 0 and 1, and when $R^2=1$ all points lie exactly on the fitted curve.

4 Results

4.1 Behavioral phenotyping

To evaluate motor function, mice were tested on the rotarod at several speeds and the latency-to-fall (LF), the time that mice spent on the rotating rod, was recorded. The stage of the disease was determined by the evaluation of animal's performance on rotarod at 10rpm (for more details see methods 3.2.2). The results obtained in the behavioral assessment of mice from both phases are summarized in table 4.I.

4.1.1 Pre-symptomatic phase

As shown in table 4.I, the mean body weight of 4-6 weeks-old SOD1(G93A) mice (18.0±0.95g, n=11) was approximately the same as WT mice (18.5±0.72g, n=16) ($p>0.05$, Student´s t test). Regarding rotarod test, the mean latency-to-fall of 4-6 weeks-old SOD1(G93A) mice did not differ from WT mice neither at 5rpm (262±14.0s, n=11, and 257±11.8, n=16, respectively, $p>0.05$, Mann Whitney test), at 10rpm (236±21.8s, n=11, and 257±11.8s, n=16, respectively, $p>0.05$, Mann Whitney test) nor at 15rpm (79.6±14.1, n=11, and 138±20.7s, n=16, respectively, $p>0.05$, Mann Whitney test), confirming the absence of symptoms in SOD1(G93A) mice at low speeds. The performance on the rotarod at 25rpm was, however, reduced in the SOD1(G93A) group (23.8±3.76s, n=11) when compared to the WT group (80.6±19.2s, n=16) ($p<0.05$, Mann Whitney test), suggesting a motor impairment at high speeds.

4.1.2 Symptomatic phase

As indicated in table 4.I, differences in the mean body weight between 12-14 weeks old SOD1(G93A) and WT mice were not detected (23.5 ± 0.93g, n=10, 23.9 ± 0.89g, n=10, in WT and SOD1 groups, $p>0.05$, Student´s t test). The performance of SOD1(G93A) mice on the rotarod task was significantly decreased when compared to WT mice. The mean latency-to-fall, not different between groups at 5rpm (267 ± 12.3s, n=10, 246 ± 23.6s n=10, in WT and SOD1(G93A) groups, $p>0.05$, Mann Whitney test), became significantly reduced by 31% at 10rpm (263±13.9s, n=10, and 181±31.3s, n=10, in WT and SOD1(G93A) groups, $p<0.05$, Mann Whitney test) 59% at 15rpm (218±20.2s, n=10, and 90.4±15.2s, n=10, in WT and SOD1(G93A) groups, $p<0.05$, Student´s t test) and 76% at 25rpm (125±28.7s, n=10, and 29.7±3.54s, n=10, in WT and SOD1(G93A) groups, $p<0.05$, Student´s t test with Welsh correction) indicating an impaired motor balance and coordination. We therefore confirmed the symptomatic state of 12-14 weeks old SOD1(G93A) mice.

Table 4.I. Motor profile of the pre-symptomatic and symptomatic SOD1(G93A) mice.

	4-6 weeks old		12-14 weeks old	
	WT	**SOD1(G93A)**	**WT**	**SOD1(G93A)**
n (mice)	16	11	10	10
Body weight (g)	18.5 ± 0.72	18.0 ± 0.95	23.5 ± 0.93	23.9 ± 0.89
LF at 5rpm (s)	242 ± 13.4	262 ± 14.0	267 ± 12.3	246 ± 23.6
LF at 10 rpm (s)	257 ± 11.8	236 ± 21.8	263 ± 13.9	181 ± 31.3$^{\#}$
LF at 15 rpm (s)	138 ± 20.7	79.6 ± 14.1	218 ± 20.2	90.4 ± 15.2*
LF at 25 rpm (s)	80.6 ± 19.2	23.8 ± 3.76$^{\#}$	125 ± 28.7	29.7 ± 3.54^{+}

The values are mean ± SEM. Results obtained from aged-matched SOD1(G93A) and WT mice were compared. (*p<0.05 for Student´s test; #p<0.05 for Mann-Whitney U-test; +p<0.05 Student´s test Welsh). LF, latency-to-fall; rpm, rotations-per-minute.

4.2 Neuromuscular transmission

4.2.1 Pre-symptomatic phase

To investigate if neuromuscular transmission is changed in the pre-symptomatic phase of ALS, we first assessed the evoked and spontaneous activity in phrenic-nerve diaphragm preparations from mice with 4-6 weeks-old.

Evoked Activity

The evoked response of pre-symptomatic SOD1(G93A) mice is presented in figure 4.1.A. As illustrated in table 4.II, pre-symptomatic SOD1(G93A) mice presented a mean amplitude of EPPs significantly higher than WT mice (15.1±1.59mV, n=25, in WT and 26.6±2.37mV, n=22, in SOD1(G93A) mice, p<0.05, Student´s t test). This difference was maintained either after normalization of muscle fiber resting membrane potential to -75mV (17.0±1.20mV, n=25, in WT and 29.5±2.14mV, n= 22, in SOD1(G93A) mice, p<0.05, Student´s t test). Similarly, the mean *quantal content* of SOD1(G93A) mice was significantly enhanced by approximately 50% in relation to WT mice (27.2±1.66, n=25, in WT and 40.7±3.09, n= 22, in SOD1(G93A) mice, p<0.05, Student´s t test with Welsh correction). As the mean resting membrane potential did not differ between WT and SOD1(G93A) mice (-68.7±2.17, n=25, and -67.0±2.67, n= 22, respectively, p>0.05, Student´s t test), these differences are not related to changes in muscle fibers viability (table 4.II).

Table 4.II. The evoked transmitter release at the diaphragm neuromuscular junctions of pre-symptomatic and symptomatic SOD1(G93A) mice.

	4-6 weeks old		12-14 weeks old	
	WT	**SOD1(G93A)**	**WT**	**SOD1(G93A)**
n (fiber, mice)	25, 13	22, 9	30, 11	39, 11
EPPs amplitude (mV)	15.1 ± 1.59	26.6 ± 2.37*	21.0 ± 2.45	18.3 ± 1.88
EPPs amplitude$_{NOR}$ (mV)	17.0 ± 1.20	29.5 ± 2.14*	23.6 ± 2.21	20.7 ± 2.00
Quantal content $_{NOR}$	27.2 ± 1.66	40.7 ± 3.09 $^{+}$	41.3 ± 3.79	35.8 ± 2.74

The values are mean ± SEM. Results obtained from age-matched SOD1(G93A) and WT mice were compared. (*p<0.05 for Student test; +p<0.05 for Student test Welsh). EPP, endplate potential; EPP_{NOR}, amplitude of endplate potential normalized to a resting membrane potential of -75mV, *Quantal content*$_{NOR}$, normalized quantal content of EPPs ($meanEPP_{NOR}/meanMEPP_{NOR}$).

Table 4.III. Passive properties and spontaneous transmitter release at the diaphragm neuromuscular junctions of pre-symptomatic and symptomatic SOD1(G93A) mice.

	4-6 weeks old		12-14 weeks old	
	WT	**SOD1(G93A)**	**WT**	**SOD1(G93A)**
n (fiber, mice)	25, 13	22, 9	30, 11	39, 11
RMP (mV)	-68.7 ± 2.17	-67.0 ± 2.67	-64.8 ± 2.50	-65.8 ± 1.69
MEPPs amplitude (mV)	0.54 ± 0.04	0.63 ± 0.03 $^{\#}$	0.50 ± 0.03	0.49 ± 0.03
MEPPs rise-time (ms)	1.17 ± 0.07	1.01 ± 0.08 $^{\#}$	0.98 ± 0.07	1.15 ± 0.07
MEPPs decay-time (ms)	3.80 ± 0.15	3.62 ± 0.18	3.12 ± 0.14	3.21 ± 0.13
MEPPs frequency (s^{-1})	0.59 ± 0.09	0.61 ± 0.10	0.76 ± 0.11	0.80 ± 0.11
NMJ with GMEPPs (n)	16	18	16	20
GMEPPs frequency (s^{-1})	0.22 ± 0.07	0.58 ± 0.13 $^{\#}$	0.44 ± 0.12	0.32 ± 0.10
Ratio	1.11 ± 0.51	2.38 ± 0.66	1.58 ± 0.49	1.21 ± 0.68

The values are mean ± SEM. Results obtained from age-matched SOD1(G93A) and WT mice were compared. (*p<0.05 for Student test; #p<0.05 for Mann-Whitney U-test; +p<0.05 for Student Welsh correction). RMP, resting membrane potential; MEPP, miniature endplate potential; NMJ, neuromuscular junction; GMEPP, giant miniature endplate potential, Ratio, GMEPPs frequency/MEPPs frequency.

Spontaneous activity

The enhancement of the neuromuscular transmission can be caused by either pre- or post-synaptic factors. To get more insights into the underlying mechanism, we looked at spontaneous events.

To evaluate a possible post-synaptic influence we looked at the amplitude of MEPPs. As indicated in table 4.II and figure 4.1, the mean amplitude of MEPPs was significantly higher in SOD1(G93A) mice by approximately 17% when compared to WT mice (0.54±0.04mV, n=25, in WT and 0.63±0.03mV, n=22, in SOD1(G93A) mice, $p<0.05$, Mann Whitney test). This difference is more outstanding when looking at the distribution of MEPPs amplitudes (figure 4.1.B) and at the Gaussian functions that shape the scatter of data (being the values for R^2, 0.92 and 0.94, in WT and SOD1(G93A) curves respectively) (figure 4.1.C). As illustrated, the SOD1(G93A) distribution presents a pronounced skewing to the right, highlighting the shift to larger amplitudes of MEPPs in this group.

Variations in the amplitudes of MEPPs can be either a consequence of post-synaptic changes in the density or kinetic properties of nicotinic ACh receptors and ACh degradation, or pre-synaptic changes, namely in the ACh content of one vesicle (quantum). In this way we next evaluated if the density or kinetic properties of nicotinic ACh receptors (mean rise-time) and enzymatic properties of acetylcholinesterase (mean decay-time) were altered in SOD1(G93A) mice. As indicated in table 4.III, SOD1(G93A) mice exhibited a mean rise-time of MEPPs significantly decreased (1.17±0.07ms, n=25, in WT and 1.01±0.08ms, n= 22, in SOD1(G93A) mice, $p<0.05$, Mann Whitney test) and no differences of the mean decay-time of MEPPs (3.80±0.15ms, n=25, in WT and 3.62±0.18ms, n= 22, in SOD1(G93A) mice, $p>0.05$, Mann Whitney test) when compared to WT mice, suggesting that the density and/or conductivity to cations of nicotinic ACh receptors is higher at SOD1(G93A) mice motor endplates.

To further evaluate a possible pre-synaptic influence we then looked at the frequency of spontaneous events. As shown in table 4.III and figure 4.1.E, the mean frequency of MEPPs in SOD1(G93A) mice (0.61±0.10s^{-1}, n=22) did not differ from WT mice (0.59±0.09s^{-1}, n=25) ($p>0.05$, Mann Whitney test). The frequency of GMEPPs was also evaluated. GMEPPs do not enter into the composition of evoked monoquantal EPPs and they are indicative of impairments in the basal levels of Ca^{2+}. As illustrated in figure 4.1.D,E and table 4.III, the presence of neuromuscular junctions exhibiting GMEPPs were more frequent in SOD1(G93A) mice (18 out of 22 neuromuscular junctions, 82%) than in WT mice (16 out of 25 neuromuscular junctions, 64%). Also, the mean frequency of GMEPPs was also significantly increase in SOD1(G93A) mice (0.58±0.13 s^{-1}, n=18) in relation to the WT mice (0.22±0.07 s^{-1}, n=16) ($p<0.05$, Mann Whitney test). To evaluate the probability of GMEPPs occurrence between groups, the mean Ratio (frequency of GMEPPs/frequency of MEPPs) was calculated for the neuromuscular junctions presenting giant events. As shown in table 4.III, the mean Ratio in SOD1(G93A) group (2.38±0.66) was increased by two folds when compared with WT group (1.11±0.51) ($p>0.05$, Mann Whitney test), suggesting that the intracellular Ca^{2+} level is higher in SOD1(G93A) mice.

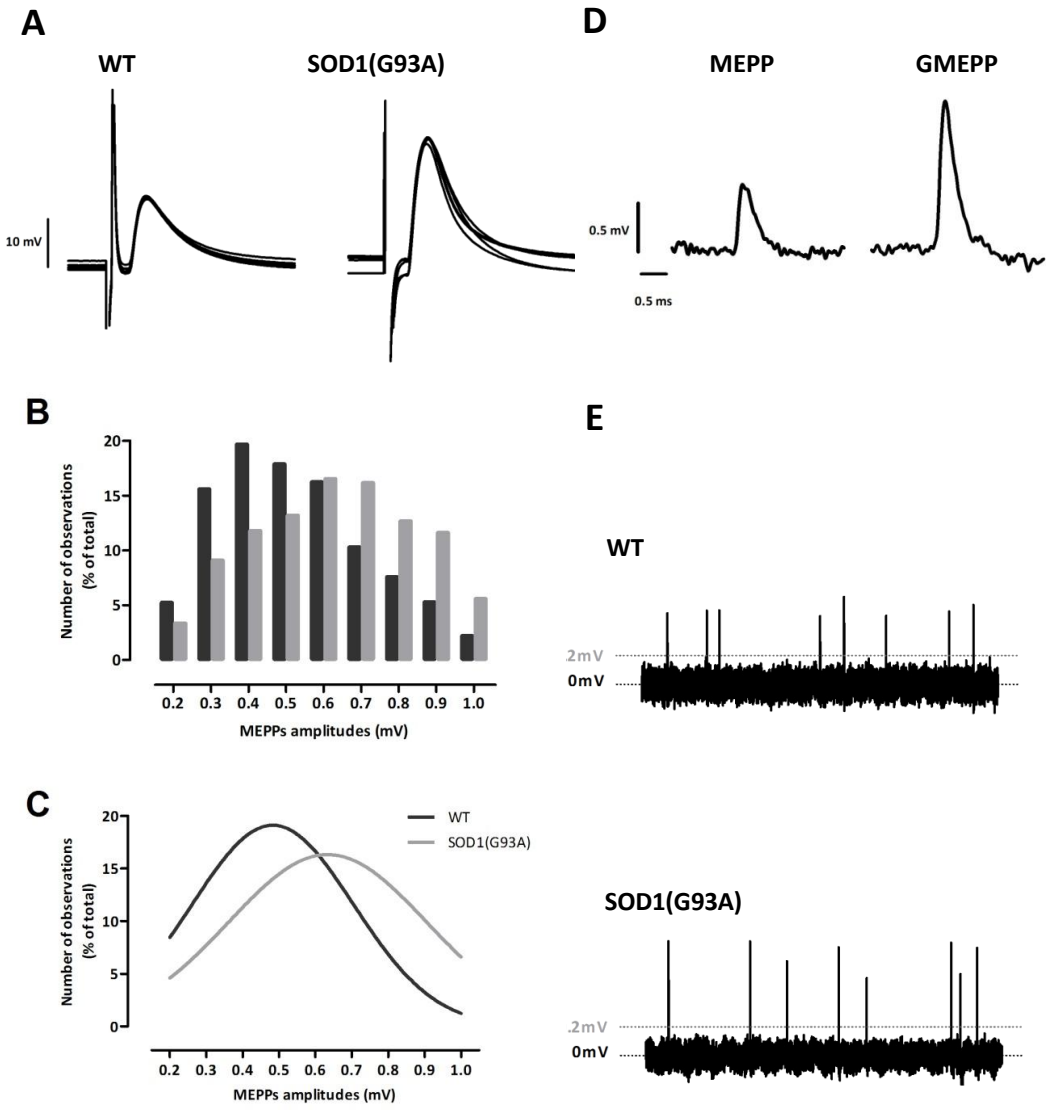

Figure 4.1 The neuromuscular transmission of the SOD1(G93A) mice in the pre-symptomatic phase of the disease.

A) Illustrates raw recordings of 5 EPPs from (4-6 weeks old) WT and pre-symptomatic SOD1(G93A) mice. B) Shows the frequency histogram of MEPPs amplitudes, which pools the amplitude of all MEPPs recorded at WT (1398 MEPPs) and SOD1(G93A) (1342 MEPPs) fibers. C) Presents the nonlinear regression applied to WT and SOD1(G93A) distributions. As illustrated, both distributions were best fitted with a Gaussian function. In D) are shown examples of a MEPP (<1mV) and a GMEPP (>1mV) and in E) examples of spontaneous events recorded in gap free mode across 10s in WT and SOD1(G93A) neuromuscular junctions.

4.2.2 Symptomatic phase

To explore if neuromuscular transmission is altered in the symptomatic phase, we also assessed the evoked and spontaneous response of phrenic-nerve diaphragm preparations from mice with 12-14 weeks-old.

Evoked Activity

The evoked response of symptomatic SOD1(G93A) mice is presented in figure 4.2. As indicated in table 4.II, symptomatic SOD1(G93A) mice revealed a slight decrease of both mean amplitude of EPPs (21.0±2.45mV, n=30, in WT and 18.3±1.88mV, n=39, in SOD1(G93A) mice, p>0.05, Mann Whitney test) and mean *quantal content* (41.3±3.79, n=30, in WT and 35.8±2.74, n=39, in SOD1(G93A) mice, p>0.05, Mann Whitney test) when comparing to WT group (table 4.II). The mean resting membrane potential was maintained between groups (-64.8±2.50, n=30, -65.8±1.69, n=39, in WT and SOD1(G93A) mice, p>0.05, Student´s t test), indicating no changes in the viability of muscle fibers (table 4.II).

Spontaneous activity

Although the evoked release of symptomatic SOD1(G93A) mice seemed to be unchanged when compared to age-matched WT mice, spontaneous activity was also studied.

As shown in table 4.III and illustrated in figure 4.2.B, the mean amplitude of MEPPs did not vary between WT and SOD1(G93A) mice (0.50±0.03mV, n=30, and 0.49±0.03mV, n= 39, respectively, p>0.05, Mann Whitney test) indicating no apparent changes in the post-synaptic cell. We noticed however, that the distribution of SOD1(G93A) MEPPs amplitudes did not follow a Gaussian distribution. Instead, a sum of two Gaussian functions best fitted the distribution of SOD1(G93A) data, shown in figure 4.2.C (first peak at 0.31±0.01 mV and second peak at 0.63±0.01mV,R^2=0.996), raising the possibility of two populations of neuromuscular junctions. To investigate this, we established the mean amplitude of SOD1(G93A) MEPPs (0.49mV) as a limit to categorize them into two groups – group A with a mean amplitude of MEPPs lower than 0.49mV and group B equal or higher than 0.49 – which will be referred to as SOD1a and SOD1b, respectively, in the following text. As illustrated in figure 4.2.D, the new distributions of MEPPs amplitudes from both groups of neuromuscular junctions were best fitted with Gaussian functions. As their peak amplitudes (Group SOD1a peak amplitude at 0.30±0.01mV, R^2=0.90, and Group SOD1b peak amplitude at 0.65±0.01mV, R^2=0.97) matched the two peak amplitudes from the bimodal curve, we could validate the grouping.

Regarding the frequency of spontaneous events, the mean frequency of MEPPs did not differ between WT and symptomatic SOD1(G93A) mice (0.76±0.11s^{-1}, n=30, and 0.80±0.11 s^{-1}, n= 39, respectively, p>0.05, Mann Whitney test). Also, SOD1(G93A) mice presented a lower number of neuromuscular junctions with GMEPPs, being the proportion reduced from approximately 53% in WT (16 out of 30 neuromuscular junctions) to 26% in SOD1(G93A) group (20 out of 39 neuromuscular junctions). The mean frequency of GMEPPs was slightly reduced by approximately 27% in SOD1(G93A) mice (0.32±0.10s^{-1}, n=20) in relation to WT mice (0.44±0.12s^{-1}, n=16) (p>0.05, Mann Whitney test). Accordingly, the mean ratio was decreased by 23% in SOD1(G93A) group (1.21±0.68, n= 39) when compared to WT mice (1.58±0.49, n=30) (p>0.05, Mann Whitney test).

Symptomatic SOD1(G93A) motor endplates

After the establishment of symptomatic SOD1(G93A) groups of neuromuscular junctions, the evoked and spontaneous parameters were re-analyzed in order to delineate the profile of each group (summarized in table 4.I). As indicated in table 4.IV, SOD1a neuromuscular junctions presented a mean amplitude of EPPs significantly reduced in relation to WT group (21.0±2.45mV, n=30, in WT and 11.4±2.00mV, n=19, in SOD1a, p<0.05, Mann Whitney test). Although the *quantal content* of EPPs was slightly decreased (41.3±3.79, n=30, in WT and 32.7±4.40, n=19, in SOD1a, p>0.05, Mann Whitney test) the statistical significance was not reached.

The mean frequency of MEPPs was approximately the same in both SOD1a and WT groups (0.76±0.11s^{-1}, n=30, and 0.61±0.11 s^{-1}, n= 19, respectively, p>0.05, Mann Whitney test). GMEPPs were, however, less frequent in SOD1a group (3 out of 19 neuromuscular junctions, 16%) than in WT (16 out of 30 neuromuscular junctions, 53%). Also, SOD1a neuromuscular junctions exhibited a lower mean frequency of GMEPPs when compared with WT group (0.44±0.12s^{-1}, n=16 in WT and 0.07±0.03 s^{-1}, n=3, in SOD1a, p<0.05) (Student t test with Welsh correction) as well as a lower mean ratio between the frequency of GMEPPs over the frequency of MEPPs (1.58±0.49, n=30, in WT and 0.11±0.07, n=3, in SOD1a) (p<0.05, Student t test with Welsh correction).

SOD1a presented a lower mean amplitude of MEPPs (0.50±0.03mV, n=30 in WT and 0.32±0.02, n= 19, in SOD1a, p<0.05, Mann Whitney test), a higher mean rise-time (0.98±0.07ms, n=30, in WT and 1.39±0.12ms, n=19, in SOD1a) (p<0.05, Mann Whitney test), and no differences in the mean decay-time of MEPPs (3.12±0.14ms, n=30, in WT and 3.12±0.17ms, n=19, in SOD1a, p>0.05, Mann Whitney test), suggesting changes in the density and/or in conductivity to cations of nicotinic ACh receptors at these SOD1(G93A) motor endplates.

Table 4.IV. The neuromuscular transmission of the two populations of neuromuscular junctions (SOD1a and SOD1b) detected in symptomatic SOD1(G93A) mice.

	12-14 weeks old		
	WT	**SOD1a**	**SOD1b**
n (fibers)	(30)	(19)	(20)
RMP (mV)	-64.8 ± 2.50	-64.4 ± 2.05	-67.1 ± 2.67
EPPs amplitude (mV)	21.0 ± 2.45	11.4 ± 2.00 #WT	24.9 ± 2.33 #SOD1a
Quantal content$_{NOR}$	41.3 ± 3.79	32.7 ± 4.40	38.8 ± 3.30
MEPPs amplitude (mV)	0.50 ± 0.03	0.32 ± 0.02 #WT	0.64 ± 0.02 #WT ; #SOD1a
MEPPs rise-time (ms)	0.98 ± 0.07	1.39 ± 0.12 #WT	0.93 ± 0.06 #SOD1a
MEPPs decay-time (ms)	3.12 ± 0.14	3.12 ± 0.17	3.28 ± 0.20
MEPPs frequency (s^{-1})	0.76 ± 0.11	0.61 ± 0.11	1.26 ± 0.33
NMJ with GMEPPs (n)	16	3	17
GMEPPs frequency (s^{-1})	0.44 ± 0.12	0.07 ± 0.03 +WT	0.38 ± 0.12 +SOD1a
Ratio	1.58 ± 0.49	0.11 ± 0.07 +WT	1.40 ± 0.80

The values are mean ± SEM. Results from SOD1a and SOD1b NMJs were compared with age-matched WT NMJs (indicated with WT symbol next to the statistical significance) and with each other (indicated with SOD1a symbol next to the statistical significance). (*p<0.05 for Student t test; #p<0.05 for M-W test; +p<0.05). RMP, resting membrane potential; EPP, endplate potential, MEPP, miniature endplate potential; GMEPP, giant miniature endplate potential; Ratio, (frequency of GMEPP)/ frequency of MEPP).

Figure 4.2 The neuromuscular transmission of the SOD1(G93A) mice in the symptomatic phase of the disease.

A) Illustrates raw recordings of 5 EPPs from symptomatic WT mice and the two groups of symptomatic SOD1(G93A) neuromuscular junctions, SOD1a and SOD1b. B) Shows the frequency histogram of MEPPs amplitudes, that pools the amplitude of all MEPPs recorded at WT (2288 events) and SOD1(G93A) (3674 events) fibers. C) Shows the nonlinear regressions that better shape WT (Gaussian function) and SOD1(G93A) (sum of two Gaussians) data. As illustrated SOD1(G93A) data follows a bimodal curve with two peak amplitudes, pointing to the existence of 2 groups of neuromuscular junctions. D) After categorizing the two groups, the distributions of MEPPs amplitudes from SOD1a and SOD1b groups were drawn and best-fitted with Gaussian functions. As it is visible, the peak amplitude from both distributions matches the two peak amplitudes from the bimodal curve, validating the grouping. E) Shows examples of spontaneous events recorded in gap free mode across 10s in WT, SOD1a and SOD1b neuromuscular junctions.

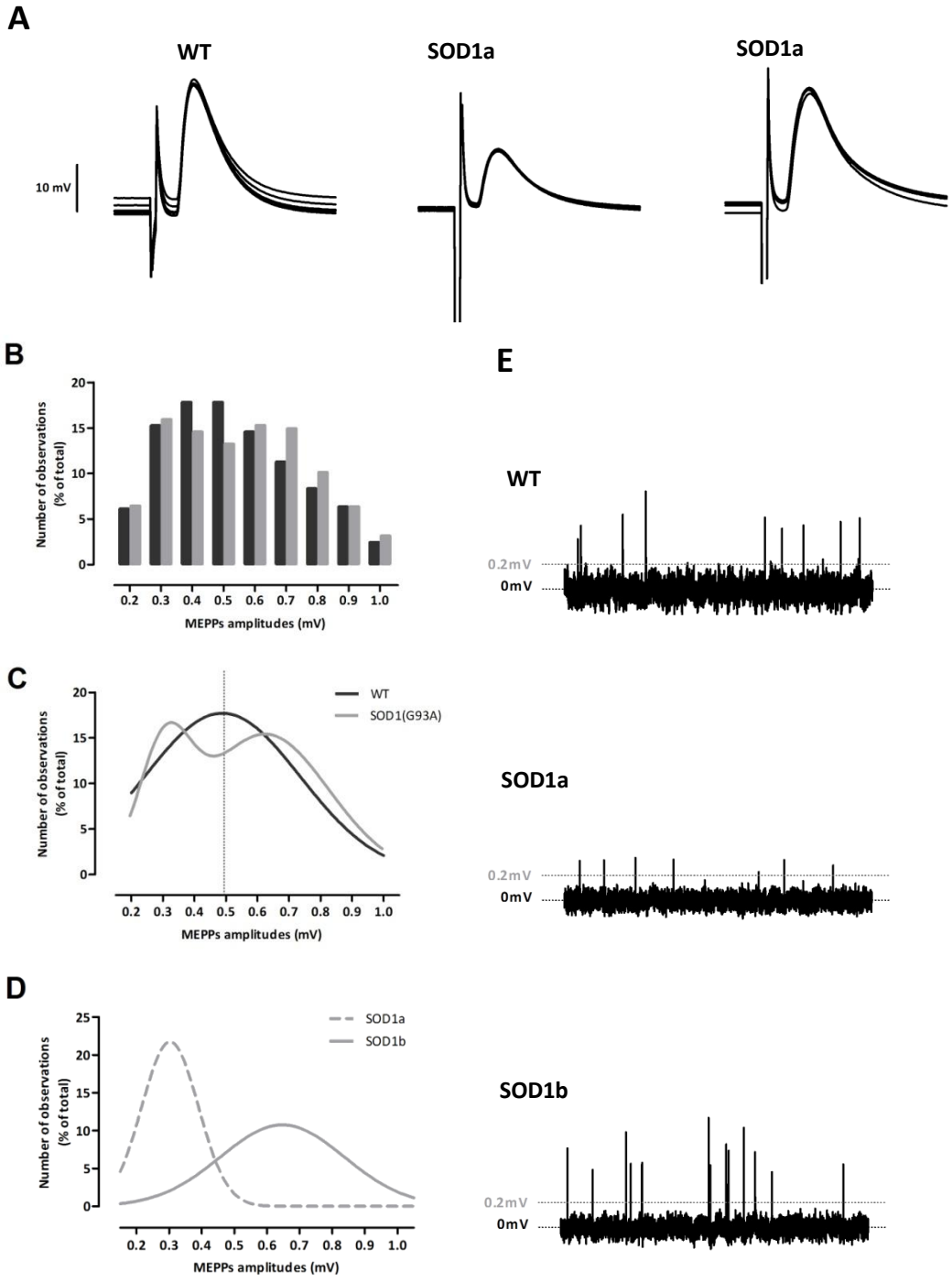
A
WT
SOD1a
SOD1a
10 mV
B
Number of observations (% of total)
MEPPs amplitudes (mV)
C
WT
SOD1(G93A)
Number of observations (% of total)
MEPPs amplitudes (mV)
D
SOD1a
SOD1b
Number of observations (% of total)
MEPPs amplitudes (mV)
E
WT
0.2mV
0mV
SOD1a
0.2mV
0mV
SOD1b
0.2mV
0mV

In contrast, SOD1b neuromuscular junctions did not show significant differences when compared to WT group in most of the parameters investigated, being the mean amplitude of MEPPs the exception. As indicated in table 4.IV, the mean amplitude of MEPPs in SOD1b was significantly higher than in WT fibers (0.50±0.03mV, n=30 in WT fibers and 0.64±0.02, n=20, in SOD1b, $p<0.05$, Mann Whitney test).

4.2.3 Comparison between phases

To clarify how the neuromuscular transmission evolved from pre-symptomatic to symptomatic SOD1(G93A) mice, from now on referred to as preSOD1(G93A) and sympSOD1(G93A) respectively, we further compared both phases of the disease.

Pre-symptomatic SOD1(G93A) vs. Symptomatic SOD1(G93A)

We first compared preSOD1(G93A) with sympSOD1(G93A) mice. This, despite disregarding the existence of two neuromuscular junction groups, shows the averaged, and so, the overall neuromuscular transmission evolution. As we can see from figures 4.3, symptomatic SOD1(G93A) mice revealed a marked reduction of the mean amplitude of EPPs (26.6±2.37mV, n=22, in preSOD1(G93A) and 18.3±1.88mV, n=39, in sympSOD1(G93A), $p<0.05$, Student t test) and no significant variation of the mean *quantal content* of EPPs ($p>0.05$, Mann Whitney test), when compared to pre-symptomatic SOD1(G93A) group. This negative trend contrasts with the positive trend from WT group which shows an increase of both mean amplitude of EPPs ($p>0.05$) and mean *quantal content* ($p<0.05$, Student t test), between these periods of time.

Regarding spontaneous activity, symptomatic SOD1(G93A) mice presented a mean amplitude of MEPPs markedly reduced (0.63±0.03mV, n=22, in preSOD1(G93A) and 0.49±0.03, n=39, in sympSOD1(G93A), $p<0.05$, Mann Whitney test) and no changes in the mean frequency of MEPPs. They revealed a slight reduced mean frequency of GMEPPs ($p>0.05$) and reduced mean ratio (2.38±0.66, n=22, in preSOD1(G93A) and 1.21±0.68, n=39, in sympSOD1(G93A), $p<0.05$, Mann Whitney test).

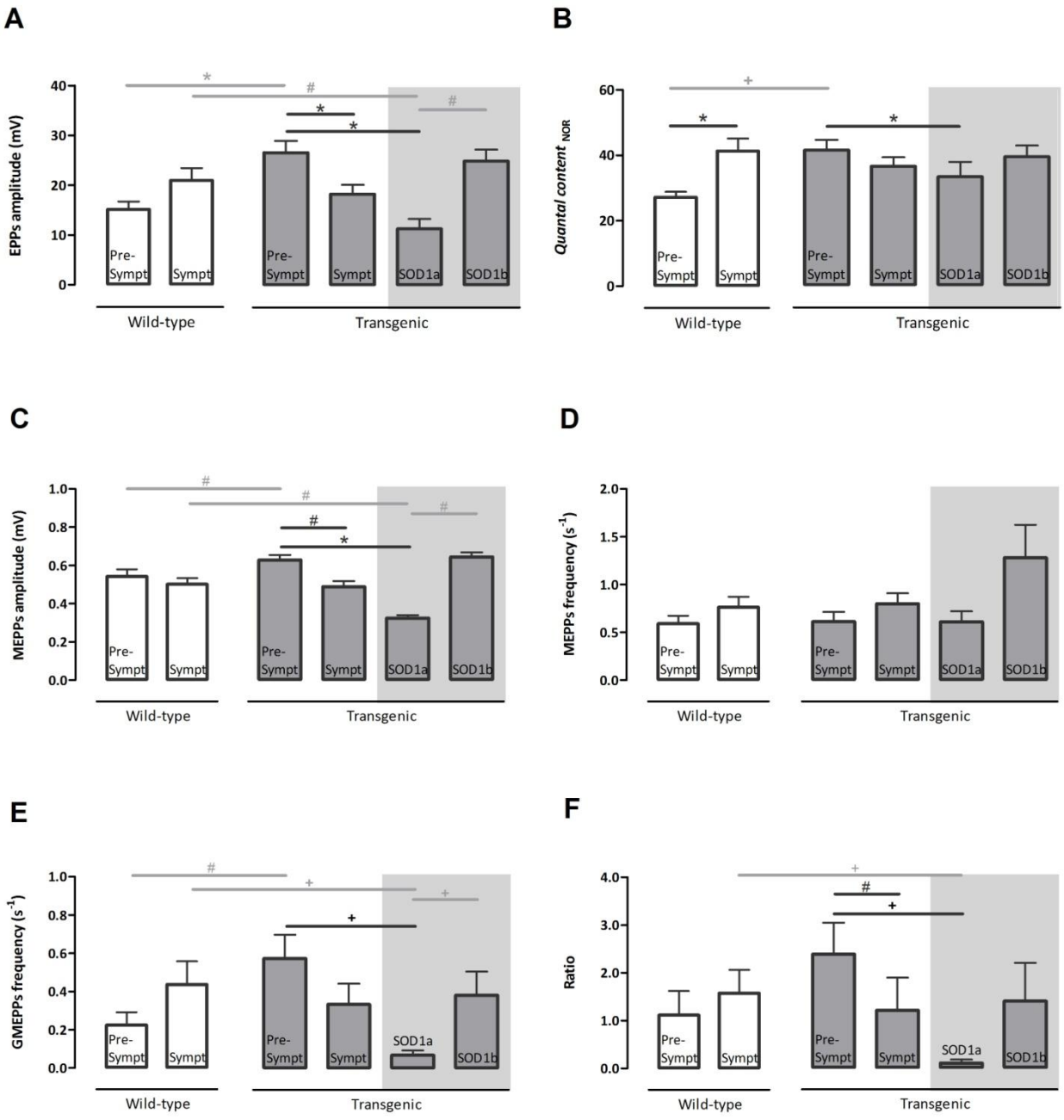

Figure 4.3 Evolution of the neuromuscular transmission from pre-symptomatic to symptomatic phases of the disease

Here is summarized the comparisons between pre-symptomatic and symptomatic WT mice (white bars) as well as pre-symptomatic and symptomatic SOD1(G93A) mice (grey bars) regarding the mean A) amplitude of EPPs, B) *quantal content*, C) amplitude of MEPPs, D) frequency of MEPPs, E) frequency of GMEPPs and F) ratio. Regarding the SOD1(G93A) mice, pre-symptomatic results were also compared to the two groups of neuromuscular junctions found in symptomatic mice (grey bars in a grey background). The significance of these comparisons, between animals from the same genotype but from different ages, are indicated in black. The comparisons done in the previous sections, between animals from different genotype but same ages, are indicated in grey. (*$p<0.05$ for Student t test; #$p<0.05$ for M-W test; +$p<0.05$).

Pre-symptomatic SOD1(G93A) vs. SOD1b

While looking at the evoked and spontaneous parameters from SOD1b group we noticed a similarity with pre-symptomatic SOD1(G93A) group. To test if these could represent the same population of neuromuscular junctions, maintained from pre-symptomatic till symptomatic phase, we then compared SOD1b to pre-symptomatic SOD1(G93A) group. Interestingly, the SOD1b neuromuscular junctions did not differ in any of the studied parameters, showing a similar electrophysiological profile to pre-symptomatic SOD1(G93A) (figure 4.3).

Pre-symptomatic SOD1(G93A) vs. SOD1a

Finally, we compared symptomatic SOD1a with pre-symptomatic SOD1(G93A) neuromuscular junctions. As shown in figure 4.3, SOD1a fibers present both mean amplitude of EPPs (26.6±2.37mV, n=22, in preSOD1, and 11.4±2.00mV, n=19, in SOD1a, $p<0.05$, Student t test) and mean *quantal content* (40.7±3.09, n=22, in preSOD1 and 32.7±4.40, n=19, in SOD1a, $p<0.05$, Student t test) significantly reduced, and no differences in the mean resting membrane potential. They also present a marked reduction of the mean amplitude of MEPPs (0.63±0.03mV, n=22, in preSOD1, and 0.32±0.02mV, n=19, in SOD1a, $p<0.05$, Mann Whitney test), as well as of the mean frequency of GMEPPs (0.58±0.13s^{-1}, n=22, in preSOD1, and 0.07±0.03s^{-1}, n=19, in SOD1a, $p<0.05$, Student t test with Welsh correction) and mean Ratio (2.38±0.66, n=22, in preSOD1, and 0.11±0.07, n=19, in SOD1a, $p<0.05$, Student t test with Welsh correction).

5 Discussion

The results reported in this work clearly show that the neuromuscular transmission of SOD1(G93A) mice presents changes along the progression of the disease. In the pre-symptomatic phase, the synaptic transmission at the phrenic-nerve diaphragm neuromuscular junction was enhanced whereas in the symptomatic phase two groups of neuromuscular junctions were detected: one group maintained the same profile as those from pre-symptomatic phase whereas in the other group, the neuromuscular transmission was compromised.

Wild-type mice neuromuscular junctions underwent normal maturation from 4-6 to 12-16 weeks-old since they showed an increase in the mean amplitude of EPPs accompanied by an increase of the mean *quantal content* of EPPs. Consistent with this, previous authors have shown that during the first weeks after birth there is a dramatic increase in the size of the motor nerve terminal (Slater 1982) which parallels with an increase in transmitter release (Diamond and Miledi 1962). Changes in the types of Ca2+ channels present at the nerve terminals also occur and were also reported to be involved in the increase of the *quantal content* of EPPs (Rosato Siri and Uchitel 1999). Furthermore, adult wild-type mice showed a reduction in both rise-time and decay-time of MEPPs. Accordingly, it is known that the maturation of nerve terminal is accompanied by a maturation of the post-synaptic membrane. During this period there is a switch in the isoform of acetylcholine receptors from γ-subunit to ε-subunit, which leads to receptors with higher conductance and shorter mean open times. This period is also characterized by the elaboration of the post-synaptic folds, with consequently a redistribution of the voltage-gated Na+ channels (Wood and Slater, 2001).

Pre-symptomatic SOD1(G93A) mice presented an enhancement of the mean amplitude of EPPs that was accompanied by an increase in the mean *quantal content* of EPPs, suggesting that more acetylcholine is being released to the synaptic cleft. These results point for an early maturation of the neuromuscular junctions in SOD1(G93A) mice since pre-symptomatic SOD1(G93A) mice and the adult wild-type mice do not present differences in the evoked activity. Therefore, this could be a compensatory response for an eventual early denervation. Accordingly, 4-6 weeks-old SOD1(G93A) mice exhibited a significant decrease of motor balance and coordination at higher speeds (25rpm) on rotarod suggesting that morphological changes like denervation and/or muscle fibers loss has already started. In line with this, previous

contractility and morphological studies in SOD1(G93A) mice also reported a decline in the number of motor units with a concomitant decline in both twitch and tetanic forces in tibialis anterior (by day 60) and gastrocnemius (by day 40) (Hegedus et al., 2008) or withdrawal of neuromuscular junctions in triceps surae gluteus and gracilis (by day 50) (Frey et al., 2000). The differences observed in the evoked activity are due to both pre- and post-synaptic mechanisms since the mean frequency of GMEPPs (associated with changes in the nerve terminal) and mean amplitude of MEPPs (associated with changes in the post-synaptic cell) were also enhanced.

Pre-symptomatic SOD1(G93A) mice showed a higher probability of synchronized spontaneous release translated by both the proportion of fibers with spontaneous "giant" events and the mean ratio between GMEPPs and MEPPs frequencies. It is known that GMEPPs are generated through a "constitutive secretion" of acetylcholine (Sellin et al., 1996), are insensitive to nerve-terminal depolarization and extracellular Ca^{2+} (Colmeus et al., 1982; Thesleff et al., 1983), being triggered by a Ca^{2+} release from intracellular stores or from an impaired processing of recycled vesicles (Rizzoli and Betz 2002). Consistent with this, SOD1(G93A) mice have (1) a defective Ca^{2+} homeostasis (Jaiswal et al., 2009), (2) present dysfunctional mitochondria in motor neurons (Kong and Xu, 1998), which have reduced ability to uptake efficiently cytoplasmatic Ca^{2+} (Vila et al., 2003; Damiano et al., 2006; Nguyen et al., 2009) and induces Ca^{2+} release from endoplasmatic reticulum stores in muscle fibers (Zhou et al., 2010). Also, (3) IgG from ALS patients were reported to interact with nerve terminals activating IP3 receptors (Pagani et al., 2006). Together, these events may cause an increase in the level of cytoplasmatic Ca^{2+} and, therefore, increase the spontaneous synchronized release of acetylcholine. GMEPPs have been reported to be enhanced under pathological conditions like paralysis (paralyzed synapses) (Gundersen 1990), nerve terminal sprouting and synapse remodeling (Miledi 1960), nerve terminals in degeneration (Birks et al., 1960) and in several motor endplate diseases (Weinstein 1980). Thus, the results described in this work suggest that diaphragm muscle from SOD1(G93A) mice already presents morphological changes in the pre-symptomatic phase. Consistent with this, Fischer and collaborators (2004) performed a spatiotemporal analysis of disease progression in SOD1(G93A) mice and they observed that 40% of end-plates were denervated at day 47. Here we show functional evidence that molecular and morphological mechanisms related to denervation might start earlier, around day 28.

SOD1(G93A) mice presented an enhancement of the mean amplitude of MEPPs in the pre-symptomatic phase that could be related to (1) an increased quantal package of transmitter through larger synaptic vesicles, (2) a decreased acetylcholinesterase activity, (3) a higher sensitivity of the muscle fiber to acetylcholine associated with higher affinity of nicotinic acetylcholine receptors to their ligand and/or higher nicotinic acetylcholine receptors expression or (4) changes in fiber type composition. To our knowledge there are no studies addressing acetylcholine content in single vesicles in ALS, although we excluded this hypothesis since SOD1(G93A) mice were reported to present ATP impairments (Mattiazzi et

al., 2002), disruption of the axonal transport (De Vos et al., 2007) and lower levels of acetylcholine transferase at nerve terminals (Tateno et al., 2009) compromising several processes such as ACh synthesis, vesicles refilling and/or recycling. We also exclude the decreased acetylcholinesterase activity since the mean decay-time of MEPPs recorded in SOD1(G93A) mice was similar to the wild-type mice, indicating that the degradation of acetylcholine is not changed in the pre-symptomatic phase of the disease. The enhancement in the mean amplitude of MEPPs could be related to changes in the expression/affinity of nicotinic acetylcholine receptors at the motor endplate. Narai and collaborators (2009) investigated the status of the neuromuscular junction along the disease progression at soleus muscle. They reported that the levels of acetylcholine receptors in SOD1(G93A) mice did not change throughout 5-20 weeks of age, and acetylcholine receptors remain clustered at neuromuscular junctions. To our knowledge there are no studies assessing acetylcholine receptors density/affinity at the diaphragm muscle in this model of ALS. However, in this work we observed that SOD1(G93A) mice present a lower rise-time of MEPPs, thereby presenting a functional evidence that pre-symptomatic SOD1(G93A) motor endplates might have a higher permeability to cations than the wild-type mice. Finally, changes in the mean amplitude of MEPPs could also be related to the muscle fiber-type composition, a finding occurring in other motor neuron diseases such as severe spinal muscular atrophy (Ruiz et al., 2010). Previous studies have shown that large motor neurons, which innervate IIB and IID/X muscle fibers, have higher vulnerability and degenerate prematurely (Hegedus et al., 2007; Hegedus et al., 2008). Moreover, pre-symptomatic SOD1(G93A) mice were shown to present a significant proportion of atrophic fast-twitch fibers (by day 60) (Atkin et al., 2005). Since the mean amplitude of MEPPs is known to be inversely related to muscle fiber diameter (Rowe and Goldspink 1969), the proportional increase of muscle fibers type IIA, which present a lower diameter, together with the increase atrophy of muscle fibers type IIB and IID/X, could explain the differences observed in the pre-symptomatic phase of the disease.

Regarding the symptomatic SOD1(G93A) mice we could find two groups of neuromuscular junctions: one (group SOD1b) maintained the same enhancement of neuromuscular transmission seen in the pre-symptomatic phase and the other (group SOD1a) presented a new profile characterized by an impairmed neuromuscular transmission (group B). Recently Naumenko and collaborators (2011) reported that the amplitude and the *quantal content* of EPPs, as well as the mean amplitude of MEPPs, recorded in symptomatic congenic SOD1(G93A) mice was not different from wild-type mice. Accordingly, if we had considered the average of all neuromuscular junctions in which recordings were performed, would achieve no differences between symptomatic SOD1(G93A) mice and wild-type mice. However, in the present study the distribution of the mean amplitude of MEPPs did not follow a normal Gaussian distribution, suggesting the presence of the above neuromuscular junctions groups. Indeed, the existence of different

neuromuscular junctions within the same muscle is commonly seen in conditions where there is a scattered temporal and spatial pattern of denervation and re-innervation processes across muscle fibers (Kretschmannova and Zemkova 2004, Ruiz et al., 2010). Consistent with this, a recent study performed by Valdez and collaborators (2012) observed that diaphragm muscle from symptomatic SOD1(G93A) mice present approximately 35% of fibers fully innervated, 20% of fibers denervated and 45% of fibers partially innervated. Moreover, in the present study some neuromuscular junctions from the symptomatic SOD1(G93A) mice presented just synchronous and asynchronous spontaneous activity and lacked an evoked response. These events have been reported to occur in other motor neuron diseases (Ruiz et al., 2010) and after axotomy (Gillingwater et al., 2002).

Neuromuscular junctions from group SOD1b presented the same profile as pre-symptomatic SOD1(G93A)mice, suggesting that, at this point, they were less affected by the disease progression. In contrast, neuromuscular junctions from SOD1a presented a significant decrease in the mean amplitude of both EPPs and MEPPs, as also a higher mean rise-time of MEPPs when compared to the wild-type mice. Altough the mean amplitude was decreased, the *quantal content* of EPPs was not significantly different, suggesting that the nerve terminal maintain its efficiency. In contrast the mean amplitude of MEPPs was reduced in the neuromuscular junctions from group SOD1a, suggesting a reduction in the influx of cations into the muscle fibers. These changes could be related to (1) a lower sensitivity of the muscle fiber to acetylcholine. Although Narai et al. (2009) did not observed changes in the levels and clusters of acetylcholine receptors in SOD1(G93A) soleus muscle, recently, Valdez and collaborators (2012), detected that neuromuscular junctions from symptomatic SOD1(G93A) EDL muscle presented post-synaptic fragmentation and decreased acetylcholine receptors density. This process has also been reported to occur during aging (Courtney and Steinbach 1981) and in other neuromuscular junction disorders such as Duchenne Muscular Dystrophy (Personius and Sawyer 2006). (2) Changes in the diaphragm muscle fibers type morphology. Accordingly, Atkin and collaborators (2005) have shown that gastronecmius muscle from SOD1(G93A) mice at the end stage presented hypertrophic slow twitch-fibers. A similar phenomena could be occurring at the diaphragm muscle as a compensatory mechanism to the ongoing denervation (3) Also, denervation/re-innervation processes which lead to an increase of the distance between the nerve terminal and the motor endplate causing a reduction in the neuromuscular junction safety factor cannot be excluded. Accordingly, during the process of aging, motor innervations is more instable (Balice-Gordon 1997).

6 Conclusions

In conclusion, the work herein reported (summarized in figure 6.1) clearly shows that the neuromuscular transmission of SOD1(G93A) mice is enhanced in the pre-symptomatic phase. This probably results from an early maturation mechanism or a compensatory response, in order to sustain an effective contraction and overcome the early denervation. In the symptomatic phase our results are consistent with the hypothesis that the diaphragm of SOD1(G93A) mice are undergoing cycles of denervation/re-innervation supported by the mixed population of neuromuscular junctions. These early changes in the neuromuscular transmission of SOD1(G93A) mice is a novel proof that the ALS associated events start long before symptoms onset. Although the evidence suggest that the impairments in the neuromuscular transmission seen in SOD1(G93A) mice are due to changes at the motor endplate level, it remains to clarify if it supports the dying-back disease hypothesis for ALS.

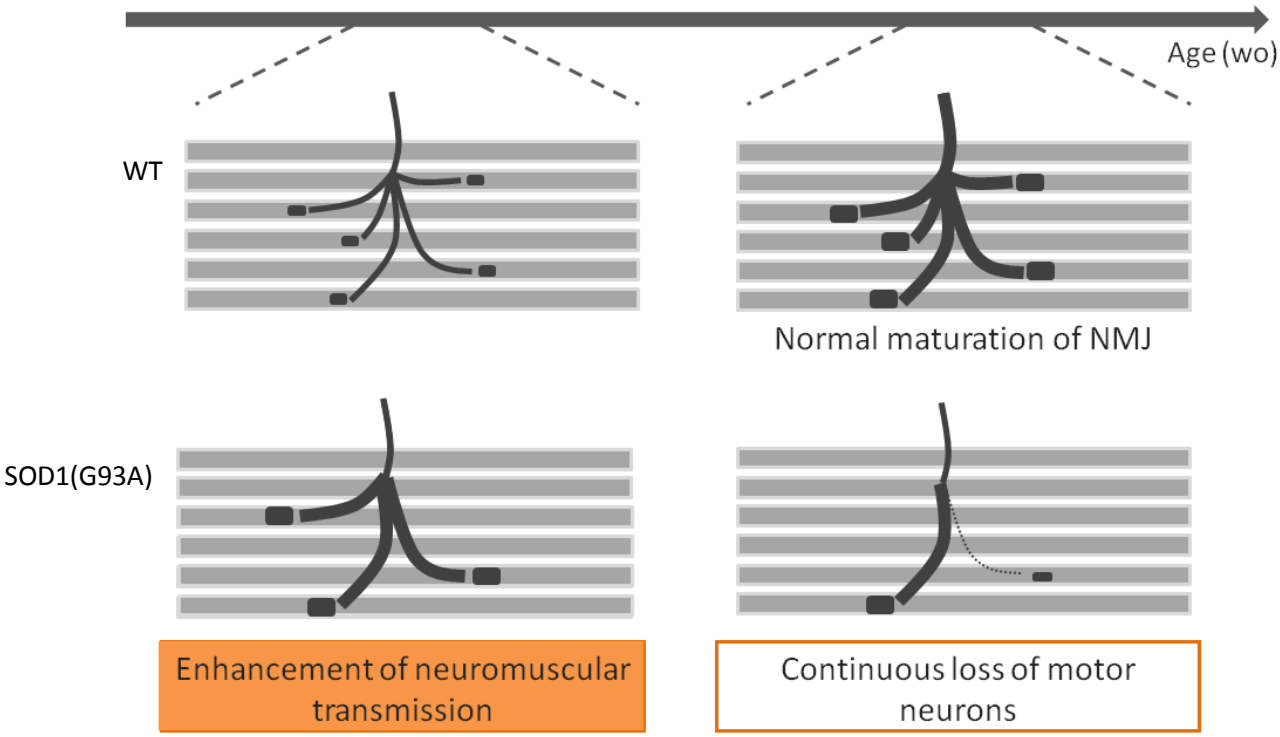

Figure 6.1 Hypothesis about the neuromuscular junctions in SOD1(G93A) along disease progression.

7 Acknowledgments

Gostaria em primeiro lugar de agradecer ao Professor Joaquim Alexandre Ribeiro e à Professora Ana Sebastião por me terem acolhido no Instituto de Neurociências e Farmacologia. Aqui pude desenvolver o meu projeto do mestrado e assim mergulhar no mundo da investigação.

Gostaria de agradecer também ao Professor Joaquim Alexandre Ribeiro, por me ter orientado e ajudado a ser rigorosa nas minhas experiências.

À Paula gostaria de agradecer-lhe pela sua importância em duas fases da minha vida. A primeira foi durante a minha licenciatura, enquanto professora da componente prática de Neurobiologia. Contagiou-me com a sua curiosidade e vontade de explorar o mundo das neurociências, incentivando sempre os alunos a terem ideias diferentes e inovadoras. Mais tarde deu-me a conhecer o mestrado em Neurociências da Faculdade de Medicina, ao qual me viria a candidatar. A segunda fase foi durante o meu mestrado, enquanto minha orientadora. Pela sua paciência em ensinar-me a técnica de eletrofisiologia, em ajudar-me a preparar os vários seminários, e em ajudar-me a organizar as minhas ideias durante a escrita da tese. Com a Paula aprendi a ser mais objetiva e concisa.

Ao Diogo Rombo, Raquel Dias e Alexandra Marçal pelas ajudas e dicas importantes que me deram, sempre que tinha problemas com o meu *setup*. Ao Jorge Valadas e Vânia Batalha por me ajudarem com o *handling* e testes comportamentais nos ratinhos. Aos meus colegas do mestrado e aos do Instituto de Neurociências e Farmacologia, porque sem eles a caminhada teria sido muito mais dura. Um obrigado especial ao Gonçalo e Filipe por trazerem mais vida ao Grupo da Junção Neuromuscular.

À minha família e amigos por terem mostrado sempre uma enorme curiosidade e interesse no meu trabalho, mesmo que lhes fosse difícil entendê-lo, essencial para me dar forças nesta caminhada.

8 References

Atkin, J. D., M. A. Farg, B. J. Turner, D. Tomas, J. A. Lysaght, J. Nunan, A. Rembach, P. Nagley, P. M. Beart, S. S. Cheema and M. K. Horne (2006). "Induction of the unfolded protein response in familial amyotrophic lateral sclerosis and association of protein-disulfide isomerase with superoxide dismutase 1." J Biol Chem **281**(40): 30152-30165.

Atkin, J. D., R. L. Scott, J. M. West, E. Lopes, A. K. Quah and S. S. Cheema (2005). "Properties of slow- and fast-twitch muscle fibres in a mouse model of amyotrophic lateral sclerosis." Neuromuscul Disord **15**(5): 377-388.

Balice-Gordon, R. J. (1997). "Age-related changes in neuromuscular innervation." Muscle Nerve Suppl **5**: S83-87.

Banerjee, R., R. L. Mosley, A. D. Reynolds, A. Dhar, V. Jackson-Lewis, P. H. Gordon, S. Przedborski and H. E. Gendelman (2008). "Adaptive immune neuroprotection in G93A-SOD1 amyotrophic lateral sclerosis mice." PLoS One **3**(7): e2740.

Bensimon, G., L. Lacomblez and V. Meininger (1994). "A controlled trial of riluzole in amyotrophic lateral sclerosis. ALS/Riluzole Study Group." N Engl J Med **330**(9): 585-591.

Birks, R., B. Katz and R. Miledi (1960). "Physiological and structural changes at the amphibian myoneural junction, in the course of nerve degeneration." J Physiol **150**: 145-168.

Boillee, S., C. Vande Velde and D. W. Cleveland (2006). "ALS: a disease of motor neurons and their nonneuronal neighbors." Neuron **52**(1): 39-59.

Boillee, S., K. Yamanaka, C. S. Lobsiger, N. G. Copeland, N. A. Jenkins, G. Kassiotis, G. Kollias and D. W. Cleveland (2006). "Onset and progression in inherited ALS determined by motor neurons and microglia." Science **312**(5778): 1389-1392.

Brooks, S. P. and S. B. Dunnett (2009). "Tests to assess motor phenotype in mice: a user's guide." Nat Rev Neurosci **10**(7): 519-529.

Brooks, V. B. and R. E. Thies (1962). "Reduction of quantum content during neuromuscular transmission." J Physiol **162**: 298-310.

Bruijn, L. I., M. W. Becher, M. K. Lee, K. L. Anderson, N. A. Jenkins, N. G. Copeland, S. S. Sisodia, J. D. Rothstein, D. R. Borchelt, D. L. Price and D. W. Cleveland (1997). "ALS-linked SOD1 mutant G85R

mediates damage to astrocytes and promotes rapidly progressive disease with SOD1-containing inclusions." Neuron **18**(2): 327-338.

Clement, A. M., M. D. Nguyen, E. A. Roberts, M. L. Garcia, S. Boillee, M. Rule, A. P. McMahon, W. Doucette, D. Siwek, R. J. Ferrante, R. H. Brown, Jr., J. P. Julien, L. S. Goldstein and D. W. Cleveland (2003). "Wild-type nonneuronal cells extend survival of SOD1 mutant motor neurons in ALS mice." Science **302**(5642): 113-117.

Colmeus, C., S. Gomez, J. Molgo and S. Thesleff (1982). "Discrepancies between spontaneous and evoked synaptic potentials at normal, regenerating and botulinum toxin poisoned mammalian neuromuscular junctions." Proc R Soc Lond B Biol Sci **215**(1198): 63-74.

Courtney, J. and J. H. Steinbach (1981). "Age changes in neuromuscular junction morphology and acetylcholine receptor distribution on rat skeletal muscle fibres." J Physiol **320**: 435-447.

Cozzolino, M., A. Ferri and M. T. Carri (2008). "Amyotrophic lateral sclerosis: from current developments in the laboratory to clinical implications." Antioxid Redox Signal **10**(3): 405-443.

Cruz, L. J., W. R. Gray, B. M. Olivera, R. D. Zeikus, L. Kerr, D. Yoshikami and E. Moczydlowski (1985). "Conus geographus toxins that discriminate between neuronal and muscle sodium channels." J Biol Chem **260**(16): 9280-9288.

Dal Canto, M. C. and M. E. Gurney (1994). "Development of central nervous system pathology in a murine transgenic model of human amyotrophic lateral sclerosis." Am J Pathol **145**(6): 1271-1279.

Damiano, M., A. A. Starkov, S. Petri, K. Kipiani, M. Kiaei, M. Mattiazzi, M. Flint Beal and G. Manfredi (2006). "Neural mitochondrial Ca2+ capacity impairment precedes the onset of motor symptoms in G93A Cu/Zn-superoxide dismutase mutant mice." J Neurochem **96**(5): 1349-1361.

De Vos, K. J., A. L. Chapman, M. E. Tennant, C. Manser, E. L. Tudor, K. F. Lau, J. Brownlees, S. Ackerley, P. J. Shaw, D. M. McLoughlin, C. E. Shaw, P. N. Leigh, C. C. Miller and A. J. Grierson (2007). "Familial amyotrophic lateral sclerosis-linked SOD1 mutants perturb fast axonal transport to reduce axonal mitochondria content." Hum Mol Genet **16**(22): 2720-2728.

Deschenes M. R., J. Covault, W. J. Kraemer and C. M. Maresh (1994). The neuromuscular junction. Muscle fibre type differences, plasticity and adaptability to increased and decreased activity. Sports Med **17**(6):358-72.

Diamond, J. and R. Miledi (1962). "A study of foetal and new-born rat muscle fibres." J Physiol **162**: 393-408.

Dion, P. A., H. Daoud and G. A. Rouleau (2009). "Genetics of motor neuron disorders: new insights into pathogenic mechanisms." Nat Rev Genet **10**(11): 769-782.

Dobrowolny, G., C. Giacinti, L. Pelosi, C. Nicoletti, N. Winn, L. Barberi, M. Molinaro, N. Rosenthal and A. Musaro (2005). "Muscle expression of a local Igf-1 isoform protects motor neurons in an ALS mouse model." J Cell Biol **168**(2): 193-199.

Dupuis, L., J. L. Gonzalez de Aguilar, F. di Scala, F. Rene, M. de Tapia, P. F. Pradat, L. Lacomblez, D. Seihlan, R. Prinjha, F. S. Walsh, V. Meininger and J. P. Loeffler (2002). "Nogo provides a molecular marker for diagnosis of amyotrophic lateral sclerosis." Neurobiol Dis **10**(3): 358-365.

Dupuis, L., J. L. Gonzalez de Aguilar, A. Echaniz-Laguna, J. Eschbach, F. Rene, H. Oudart, B. Halter, C. Huze, L. Schaeffer, F. Bouillaud and J. P. Loeffler (2009). "Muscle mitochondrial uncoupling dismantles neuromuscular junction and triggers distal degeneration of motor neurons." PLoS One **4**(4): e5390.

Dupuis, L., H. Oudart, F. Rene, J. L. Gonzalez de Aguilar and J. P. Loeffler (2004). "Evidence for defective energy homeostasis in amyotrophic lateral sclerosis: benefit of a high-energy diet in a transgenic mouse model." Proc Natl Acad Sci U S A **101**(30): 11159-11164.

Elliott, J. L. (2001). "Cytokine upregulation in a murine model of familial amyotrophic lateral sclerosis." Brain Res Mol Brain Res **95**(1-2): 172-178.

Fatt, P. and B. Katz (1952). "Spontaneous subthreshold activity at motor nerve endings." J Physiol **117**(1): 109-128.

Fischer, L. R., D. G. Culver, P. Tennant, A. A. Davis, M. Wang, A. Castellano-Sanchez, J. Khan, M. A. Polak and J. D. Glass (2004). "Amyotrophic lateral sclerosis is a distal axonopathy: evidence in mice and man." Exp Neurol **185**(2): 232-240.

Frey, D., C. Schneider, L. Xu, J. Borg, W. Spooren and P. Caroni (2000). "Early and selective loss of neuromuscular synapse subtypes with low sprouting competence in motoneuron diseases." J Neurosci **20**(7): 2534-2542.

Gillingwater, T. H., D. Thomson, T. G. Mack, E. M. Soffin, R. J. Mattison, M. P. Coleman and R. R. Ribchester (2002). "Age-dependent synapse withdrawal at axotomised neuromuscular junctions in Wld(s) mutant and Ube4b/Nmnat transgenic mice." J Physiol **543**(Pt 3): 739-755.

Giniatullin, A. R., F. Darios, A. Shakirzyanova, B. Davletov and R. Giniatullin (2006). "SNAP25 is a pre-synaptic target for the depressant action of reactive oxygen species on transmitter release." J Neurochem **98**(6): 1789-1797.

Giniatullin, A. R. and R. A. Giniatullin (2003). "Dual action of hydrogen peroxide on synaptic transmission at the frog neuromuscular junction." J Physiol **552**(Pt 1): 283-293.

Gong, Y. H., A. S. Parsadanian, A. Andreeva, W. D. Snider and J. L. Elliott (2000). "Restricted expression of G86R Cu/Zn superoxide dismutase in astrocytes results in astrocytosis but does not cause motoneuron degeneration." J Neurosci **20**(2): 660-665.

Gonzalez de Aguilar, J. L., A. Echaniz-Laguna, A. Fergani, F. Rene, V. Meininger, J. P. Loeffler and L. Dupuis (2007). "Amyotrophic lateral sclerosis: all roads lead to Rome." J Neurochem **101**(5): 1153-1160.

Gonzalez, L. E., M. L. Kotler, L. G. Vattino, E. Conti, R. C. Reisin, K. J. Mulatz, T. P. Snutch and O. D. Uchitel (2011). "Amyotrophic lateral sclerosis-immunoglobulins selectively interact with neuromuscular junctions expressing P/Q-type calcium channels." J Neurochem **119**(4): 826-838.

Gundersen, K. (1990). "Spontaneous activity at long-term silenced synapses in rat muscle." J Physiol **430**: 399-418.

Gurney, M. E., H. Pu, A. Y. Chiu, M. C. Dal Canto, C. Y. Polchow, D. D. Alexander, J. Caliendo, A. Hentati, Y. W. Kwon, H. X. Deng and et al. (1994). "Motor neuron degeneration in mice that express a human Cu,Zn superoxide dismutase mutation." Science **264**(5166): 1772-1775.

Hall, E. D., J. A. Oostveen and M. E. Gurney (1998). "Relationship of microglial and astrocytic activation to disease onset and progression in a transgenic model of familial ALS." Glia **23**(3): 249-256.

Hegedus, J., C. T. Putman and T. Gordon (2007). "Time course of preferential motor unit loss in the SOD1 G93A mouse model of amyotrophic lateral sclerosis." Neurobiol Dis **28**(2): 154-164.

Hegedus, J., C. T. Putman, N. Tyreman and T. Gordon (2008). "Preferential motor unit loss in the SOD1 G93A transgenic mouse model of amyotrophic lateral sclerosis." J Physiol **586**(14): 3337-3351.

Hensley, K., J. Fedynyshyn, S. Ferrell, R. A. Floyd, B. Gordon, P. Grammas, L. Hamdheydari, M. Mhatre, S. Mou, Q. N. Pye, C. Stewart, M. West, S. West and K. S. Williamson (2003). "Message and protein-level elevation of tumor necrosis factor alpha (TNF alpha) and TNF alpha-modulating cytokines in spinal cords of the G93A-SOD1 mouse model for amyotrophic lateral sclerosis." Neurobiol Dis **14**(1): 74-80.

Higgins, C. M., C. Jung and Z. Xu (2003). "ALS-associated mutant SOD1G93A causes mitochondrial vacuolation by expansion of the intermembrane space and by involvement of SOD1 aggregation and peroxisomes." BMC Neurosci **4**: 16.

Hubert, J. P., J. C. Delumeau, J. Glowinski, J. Premont and A. Doble (1994). "Antagonism by riluzole of entry of calcium evoked by NMDA and veratridine in rat cultured granule cells: evidence for a dual mechanism of action." Br J Pharmacol **113**(1): 261-267.

Jaiswal, M. K., W. D. Zech, M. Goos, C. Leutbecher, A. Ferri, A. Zippelius, M. T. Carri, R. Nau and B. U. Keller (2009). "Impairment of mitochondrial calcium handling in a mtSOD1 cell culture model of motoneuron disease." BMC Neurosci **10**: 64.

Julien, J. P. and J. Kriz (2006). "Transgenic mouse models of amyotrophic lateral sclerosis." Biochim Biophys Acta **1762**(11-12): 1013-1024.

Kabashi, E., J. N. Agar, D. M. Taylor, S. Minotti and H. D. Durham (2004). "Focal dysfunction of the proteasome: a pathogenic factor in a mouse model of amyotrophic lateral sclerosis." J Neurochem **89**(6): 1325-1335.

Kandel E.R., J. H. Schwartz and T. M. Jessell (2000). Principles of Neural Science, 4th edition. McGraw-Hill, New York.

Kato, S. (2008). "Amyotrophic lateral sclerosis models and human neuropathology: similarities and differences." Acta Neuropathol 115(1): 97-114.

Kawamata, H. and G. Manfredi (2010). "Mitochondrial dysfunction and intracellular calcium dysregulation in ALS." Mech Ageing Dev **131**(7-8): 517-526.

Kiernan, M. C., S. Vucic, B. C. Cheah, M. R. Turner, A. Eisen, O. Hardiman, J. R. Burrell and M. C. Zoing (2011). "Amyotrophic lateral sclerosis." Lancet **377**(9769): 942-955.

Kim, H. J., M. Kim, S. H. Kim, J. J. Sung and K. W. Lee (2002). "Alteration in intracellular calcium homeostasis reduces motor neuronal viability expressing mutated Cu/Zn superoxide dismutase through a nitric oxide/guanylyl cyclase cGMP cascade." Neuroreport **13**(9): 1131-1135.

Kim, Y. I., C. Joo, C. C. Cheng, C. E. Davis and T. J. O´Shaughnessy (1996). Neuromuscular transmission in a transgenic model of motor neuron disease. 18th Annual International Conference of the IEEE Engineering in Medicine and Biology Society, Amsterdam.

Knippenberg, S., N. Thau, R. Dengler and S. Petri (2010). "Significance of behavioural tests in a transgenic mouse model of amyotrophic lateral sclerosis (ALS)." Behav Brain Res **213**(1): 82-87.

Kong, J. and Z. Xu (1998). "Massive mitochondrial degeneration in motor neurons triggers the onset of amyotrophic lateral sclerosis in mice expressing a mutant SOD1." J Neurosci **18**(9): 3241-3250.

Kretschmannova, K. and H. Zemkova (2004). "Characterization of neuromuscular transmission in mice with progressive motoneuronopathy." Physiol Res **53**(5): 541-548.

Kuffler, S. W. and D. Yoshikami (1975). "The number of transmitter molecules in a quantum: an estimate from iontophoretic application of acetylcholine at the neuromuscular synapse." J Physiol **251**(2): 465-482.

Liley, A. W. (1957). "Spontaneous release of transmitter substance in multiquantal units." J Physiol **136**(3): 595-605.

Malgouris, C., M. Daniel and A. Doble (1994). "Neuroprotective effects of riluzole on N-methyl-D-aspartate- or veratridine-induced neurotoxicity in rat hippocampal slices." Neurosci Lett **177**(1-2): 95-99.

Mantilla, C. B. and G. C. Sieck (2009). "Neuromuscular adaptations to respiratory muscle inactivity." Respir Physiol Neurobiol **169**(2): 133-140.

Marcuzzo, S., I. Zucca, A. Mastropietro, N. K. de Rosbo, P. Cavalcante, S. Tartari, S. Bonanno, L. Preite, R. Mantegazza and P. Bernasconi (2011). "Hind limb muscle atrophy precedes cerebral neuronal degeneration in G93A-SOD1 mouse model of amyotrophic lateral sclerosis: a longitudinal MRI study." Exp Neurol **231**(1): 30-37.

Maselli, R. A., R. L. Wollman, C. Leung, B. Distad, S. Palombi, D. P. Richman, E. F. Salazar-Grueso and R. P. Roos (1993). "Neuromuscular transmission in amyotrophic lateral sclerosis." Muscle Nerve **16**(11): 1193-1203.

Mattiazzi, M., M. D'Aurelio, C. D. Gajewski, K. Martushova, M. Kiaei, M. F. Beal and G. Manfredi (2002). "Mutated human SOD1 causes dysfunction of oxidative phosphorylation in mitochondria of transgenic mice." J Biol Chem **277**(33): 29626-29633.

Miledi, R. (1960). "Properties of regenerating neuromuscular synapses in the frog." J Physiol **154**: 190-205.

Miller, R. G., J. D. Mitchell, M. Lyon and D. H. Moore (2003). "Riluzole for amyotrophic lateral sclerosis (ALS)/motor neuron disease (MND)." Amyotroph Lateral Scler Other Motor Neuron Disord **4**(3): 191-206.

Mizoule, J., B. Meldrum, M. Mazadier, M. Croucher, C. Ollat, A. Uzan, J. J. Legrand, C. Gueremy and G. Le Fur (1985). "2-Amino-6-trifluoromethoxy benzothiazole, a possible antagonist of excitatory amino acid neurotransmission--I. Anticonvulsant properties." Neuropharmacology **24**(8): 767-773.

Monville, C., E. M. Torres and S. B. Dunnett (2006). "Comparison of incremental and accelerating protocols of the rotarod test for the assessment of motor deficits in the 6-OHDA model." J Neurosci Methods **158**(2): 219-223.

Naguib, M., P. Flood, J. J. McArdle and H. R. Brenner (2002). "Advances in neurobiology of the neuromuscular junction: implications for the anesthesiologist." Anesthesiology **96**(1): 202-231.

Narai, H., Y. Manabe, M. Nagai, I. Nagano, Y. Ohta, T. Murakami, Y. Takehisa, T. Kamiya and K. Abe (2009). "Early detachment of neuromuscular junction proteins in ALS mice with SODG93A mutation." Neurol Int **1**(1): e16.

Naumenko, N., E. Pollari, A. Kurronen, R. Giniatullina, A. Shakirzyanova, J. Magga, J. Koistinaho and R. Giniatullin (2011). "Gender-Specific Mechanism of Synaptic Impairment and Its Prevention by GCSF in a Mouse Model of ALS." Front Cell Neurosci **5**: 26.

Naves, L. A. and W. Van der Kloot (2001). "Repetitive nerve stimulation decreases the acetylcholine content of quanta at the frog neuromuscular junction." J Physiol **532**(Pt 3): 637-647.

Nguyen, K. T., L. E. Garcia-Chacon, J. N. Barrett, E. F. Barrett and G. David (2009). "The Psi(m) depolarization that accompanies mitochondrial Ca2+ uptake is greater in mutant SOD1 than in wild-type mouse motor terminals." Proc Natl Acad Sci U S A **106**(6): 2007-2011.

O'Shaughnessy, T. J., H. Yan, J. Kim, E. H. Middlekauff, K. W. Lee, L. H. Phillips and Y. I. Kim (1998). "Amyotrophic lateral sclerosis: serum factors enhance spontaneous and evoked transmitter release at the neuromuscular junction." Muscle Nerve **21**(1): 81-90.

Pagani, M. R., R. C. Reisin and O. D. Uchitel (2006). "Calcium signaling pathways mediating synaptic potentiation triggered by amyotrophic lateral sclerosis IgG in motor nerve terminals." J Neurosci **26**(10): 2661-2672.

Pardo, N. E., R. K. Hajela and W. D. Atchison (2006). "Acetylcholine release at neuromuscular junctions of adult tottering mice is controlled by N-(cav2.2) and R-type (cav2.3) but not L-type (cav1.2) Ca2+ channels." J Pharmacol Exp Ther **319**(3): 1009-1020.

Personius, K. E. and R. P. Sawyer (2006). "Variability and failure of neurotransmission in the diaphragm of mdx mice." Neuromuscul Disord **16**(3): 168-177.

Pousinha, P.A., A. M. Correia, A. M. Sebastiao and J. A. Ribeiro (2012). Neuromuscular transmission modulation by adenosine upon aging. Neurobiol Aging

Pramatarova, A., J. Laganiere, J. Roussel, K. Brisebois and G. A. Rouleau (2001). "Neuron-specific expression of mutant superoxide dismutase 1 in transgenic mice does not lead to motor impairment." J Neurosci **21**(10): 3369-3374.

Pun, S., A. F. Santos, S. Saxena, L. Xu and P. Caroni (2006). "Selective vulnerability and pruning of phasic motoneuron axons in motoneuron disease alleviated by CNTF." Nat Neurosci **9**(3): 408-419.

Purves D., G. J. Augustine, D. Fitzpatrick et al., editors (2001). Neuroscience. 2nd edition. Sunderland (MA): Sinauer Associates.

Raoul, C., A. G. Estevez, H. Nishimune, D. W. Cleveland, O. deLapeyriere, C. E. Henderson, G. Haase and B. Pettmann (2002). "Motoneuron death triggered by a specific pathway downstream of Fas. potentiation by ALS-linked SOD1 mutations." Neuron **35**(6): 1067-1083.

Reaume, A. G., J. L. Elliott, E. K. Hoffman, N. W. Kowall, R. J. Ferrante, D. F. Siwek, H. M. Wilcox, D. G. Flood, M. F. Beal, R. H. Brown, Jr., R. W. Scott and W. D. Snider (1996). "Motor neurons in Cu/Zn superoxide dismutase-deficient mice develop normally but exhibit enhanced cell death after axonal injury." Nat Genet **13**(1): 43-47.

Ribeiro, J. A. and A. M. Sebastião (1987). On the role, inactivation and origin of endogenous adenosine at the frog neuromuscular junction. J Physiol **384**:571-585.

Ribeiro, JA and J. Walker (1975). The effects of adenosine triphosphate and adenosine diphosphate on transmission at the rat and frog neuromuscular junctions. Br J Pharmacol **54**:213-218.

Richards, D.A., C. Guatimosim, S. O. Rizzoli and W. J. Betz (2003). Synaptic vesicle pools at the frog neuromuscular junction. Neuron 39:529-541.

Ripps, M. E., G. W. Huntley, P. R. Hof, J. H. Morrison and J. W. Gordon (1995). "Transgenic mice expressing an altered murine superoxide dismutase gene provide an animal model of amyotrophic lateral sclerosis." Proc Natl Acad Sci U S A **92**(3): 689-693.

Rizzoli, S. O. and W. J. Betz (2002). "Effects of 2-(4-morpholinyl)-8-phenyl-4H-1-benzopyran-4-one on synaptic vesicle cycling at the frog neuromuscular junction." J Neurosci **22**(24): 10680-10689.

Rizzoli, S. O. and W. J. Betz (2005). "Synaptic vesicle pools." Nat Rev Neurosci **6**(1): 57-69.

Rosato Siri, M. D. and O. D. Uchitel (1999). "Calcium channels coupled to neurotransmitter release at neonatal rat neuromuscular junctions." J Physiol **514 (Pt 2)**: 533-540.

Rosen, D. R., T. Siddique, D. Patterson, D. A. Figlewicz, P. Sapp, A. Hentati, D. Donaldson, J. Goto, J. P. O'Regan, H. X. Deng and et al. (1993). "Mutations in Cu/Zn superoxide dismutase gene are associated with familial amyotrophic lateral sclerosis." Nature **362**(6415): 59-62.

Rowe, R. W. and G. Goldspink (1969). "Muscle fibre growth in five different muscles in both sexes of mice." J Anat **104**(Pt 3): 519-530.

Rozas, G., M. J. Guerra and J. L. Labandeira-Garcia (1997). "An automated rotarod method for quantitative drug-free evaluation of overall motor deficits in rat models of parkinsonism." Brain Res Brain Res Protoc **2**(1): 75-84.

Rozas, J. L., L. Gomez-Sanchez, C. Tomas-Zapico, J. J. Lucas and R. Fernandez-Chacon (2011). "Increased neurotransmitter release at the neuromuscular junction in a mouse model of polyglutamine disease." J Neurosci **31**(3): 1106-1113.

Ruiz, R., J. J. Casanas, L. Torres-Benito, R. Cano and L. Tabares (2010). "Altered intracellular Ca2+ homeostasis in nerve terminals of severe spinal muscular atrophy mice." J Neurosci **30**(3): 849-857.

Schiffer, D., S. Cordera, P. Cavalla and A. Migheli (1996). "Reactive astrogliosis of the spinal cord in amyotrophic lateral sclerosis." J Neurol Sci **139 Suppl**: 27-33.

Sellin, L. C., J. Molgo, K. Tornquist, B. Hansson and S. Thesleff (1996). "On the possible origin of giant or slow-rising miniature end-plate potentials at the neuromuscular junction." Pflugers Arch **431**(3): 325-334.

Shaw, P. J., P. G. Ince, G. Falkous and D. Mantle (1995). "Oxidative damage to protein in sporadic motor neuron disease spinal cord." Ann Neurol **38**(4): 691-695.

Siklos, L., J. I. Engelhardt, M. E. Alexianu, M. E. Gurney, T. Siddique and S. H. Appel (1998). "Intracellular calcium parallels motoneuron degeneration in SOD-1 mutant mice." J Neuropathol Exp Neurol **57**(6): 571-587.

Simpson, E. P., Y. K. Henry, J. S. Henkel, R. G. Smith and S. H. Appel (2004). "Increased lipid peroxidation in sera of ALS patients: a potential biomarker of disease burden." Neurology **62**(10): 1758-1765.

Slater, C. R. (1982). "Postnatal maturation of nerve-muscle junctions in hindlimb muscles of the mouse." Dev Biol **94**(1): 11-22.

Smittkamp, S. E., J. W. Brown and J. A. Stanford (2008). "Time-course and characterization of orolingual motor deficits in B6SJL-Tg(SOD1-G93A)1Gur/J mice." Neuroscience **151**(2): 613-621.

Sons, M. S. and J. J. Plomp (2006). "Rab3A deletion selectively reduces spontaneous neurotransmitter release at the mouse neuromuscular synapse." Brain Res **1089**(1): 126-134.

Souayah, N., K. M. Coakley, R. Chen, N. Ende and J. J. McArdle (2012). "Defective neuromuscular transmission in the SOD1 G93A transgenic mouse improves after administration of human umbilical cord blood cells." Stem Cell Rev **8**(1): 224-228.

Swarup, V. and J. P. Julien (2011). "ALS pathogenesis: recent insights from genetics and mouse models." Prog Neuropsychopharmacol Biol Psychiatry **35**(2): 363-369.

Tateno, M., S. Kato, T. Sakurai, N. Nukina, R. Takahashi and T. Araki (2009). "Mutant SOD1 impairs axonal transport of choline acetyltransferase and acetylcholine release by sequestering KAP3." Hum Mol Genet **18**(5): 942-955.

Thesleff, S., J. Molgo and H. Lundh (1983). "Botulinum toxin and 4-aminoquinoline induce a similar abnormal type of spontaneous quantal transmitter release at the rat neuromuscular junction." Brain Res **264**(1): 89-97.

Turner, B. J. and K. Talbot (2008). "Transgenics, toxicity and therapeutics in rodent models of mutant SOD1-mediated familial ALS." Prog Neurobiol **85**(1): 94-134.

Uchitel, O. D., S. H. Appel, F. Crawford and L. Sczcupak (1988). "Immunoglobulins from amyotrophic lateral sclerosis patients enhance spontaneous transmitter release from motor-nerve terminals." Proc Natl Acad Sci U S A **85**(19): 7371-7374.

Uchitel, O. D., F. Scornik, D. A. Protti, C. G. Fumberg, V. Alvarez and S. H. Appel (1992). "Long-term neuromuscular dysfunction produced by passive transfer of amyotrophic lateral sclerosis immunoglobulins." Neurology **42**(11): 2175-2180.

Urushitani, M., J. Kurisu, K. Tsukita and R. Takahashi (2002). "Proteasomal inhibition by misfolded mutant superoxide dismutase 1 induces selective motor neuron death in familial amyotrophic lateral sclerosis." J Neurochem **83**(5): 1030-1042.

Valdez, G., J. C. Tapia, J. W. Lichtman, M. A. Fox and J. R. Sanes (2012). "Shared resistance to aging and ALS in neuromuscular junctions of specific muscles." PLoS One **7**(4): e34640.

Vila, L., E. F. Barrett and J. N. Barrett (2003). "Stimulation-induced mitochondrial [Ca2+] elevations in mouse motor terminals: comparison of wild-type with SOD1-G93A." J Physiol **549**(Pt 3): 719-728.

Vos, M., E. Lauwers and P. Verstreken (2010). "Synaptic mitochondria in synaptic transmission and organization of vesicle pools in health and disease." Front Synaptic Neurosci **2**: 139.

Weinstein, S. P. (1980). "A comparative electrophysiological study of motor end-plate diseased skeletal muscle in the mouse." J Physiol **307**: 453-464.

Wengenack, T. M., S. S. Holasek, C. M. Montano, D. Gregor, G. L. Curran and J. F. Poduslo (2004). "Activation of programmed cell death markers in ventral horn motor neurons during early presymptomatic stages of amyotrophic lateral sclerosis in a transgenic mouse model." Brain Res **1027**(1-2): 73-86.

Wiedemann, F. R., G. Manfredi, C. Mawrin, M. F. Beal and E. A. Schon (2002). "Mitochondrial DNA and respiratory chain function in spinal cords of ALS patients." J Neurochem **80**(4): 616-625.

Williamson, T. L. and D. W. Cleveland (1999). "Slowing of axonal transport is a very early event in the toxicity of ALS-linked SOD1 mutants to motor neurons." Nat Neurosci **2**(1): 50-56.

Wong, M. and L. J. Martin (2010). "Skeletal muscle-restricted expression of human SOD1 causes motor neuron degeneration in transgenic mice." Hum Mol Genet **19**(11): 2284-2302.

Wong, P. C., C. A. Pardo, D. R. Borchelt, M. K. Lee, N. G. Copeland, N. A. Jenkins, S. S. Sisodia, D. W. Cleveland and D. L. Price (1995). "An adverse property of a familial ALS-linked SOD1 mutation causes motor neuron disease characterized by vacuolar degeneration of mitochondria." Neuron **14**(6): 1105-1116.

Wood, S. J. and C. R. Slater (2001). "Safety factor at the neuromuscular junction." Prog Neurobiol **64**(4): 393-429.

Zhang, B., P. Tu, F. Abtahian, J. Q. Trojanowski and V. M. Lee (1997). "Neurofilaments and orthograde transport are reduced in ventral root axons of transgenic mice that express human SOD1 with a G93A mutation." J Cell Biol **139**(5): 1307-1315.

Zhou, J., J. Yi, R. Fu, E. Liu, T. Siddique, E. Rios and H. X. Deng (2010). "Hyperactive intracellular calcium signaling associated with localized mitochondrial defects in skeletal muscle of an animal model of amyotrophic lateral sclerosis." J Biol Chem **285**(1): 705-712.